# Authors' Response to Reviews of

# NMVOC emission optimization in China through assimilating formaldehyde retrievals from multiple satellite products

Canjie Xu[1], Jianbing Jin*[1], Ke Li[1], Yinfei Qi[2], Ji Xia[1], Hai Xiang Lin[3,4], Hong Liao[1]
*Atmospheric Chemistry and Physics,* 10.5194/egusphere-2025-140

**RC:** ***Reviewers' Comment***, AR: Authors' Response, □ Manuscript Text

## 1. Overview

Response to Referee 1: We would like to thank the referee for the careful review throughout the paper and the in-depth comments, especially for the way we processed the formaldehyde column observations which was improper. We accepted all of the referee's suggestion for using the satellite formaldehyde retrievals. The posterior results now also differ from the previous results significantly. Because there are too many modifications throughout the manuscript, we did not highlight all of them.

## 2. Major concerns

**RC:** ***1) Clarity and Consistency in Satellite Usage (Major) The manuscript lacks consistency in describing which satellite datasets are assimilated and which are used for validation. The abstract suggests that only OMPS is used for assimilation and TROPOMI is used as an independent validation dataset. However, the methods section refers to assimilation experiments involving OMPS, TROPOMI, and their combination. Furthermore, Eq. (3) implies the use of a single observational constraint. If the combination refers to an average of OMPS and TROPOMI data, this should be clearly stated and methodologically justified. Averaging observations reduces variance and effectively increases their weight in the cost function-this is not equivalent to joint multi-satellite assimilation. This distinction must be clarified and its implications explicitly discussed.***

AR: We express our gratitude to the reviewer for highlighting the inconsistency in our description of the satellite datasets used for assimilation and validation. We acknowledge that the "OMPS+TROPOMI combined assimilation" approach in the original submission was inadequately described and methodologically flawed. As the reviewer accurately pointed out, simply averaging OMPS and TROPOMI retrievals does not constitute true multi-satellite joint assimilation, as it artificially reduces observational variance and disproportionately weights the cost function without properly accounting for observational errors. In the revised manuscript, we have removed the combined assimilation experiment entirely, focusing solely on the OMPS-only and TROPOMI-only assimilation experiments. We have ensured consistent descriptions throughout the Abstract, Methods, and Results sections to eliminate ambiguity. Additionally, we have introduced a consistency analysis in the Results section to highlight the benefit of using the TROPOMI-based and OMPS-based assimilation results, and details could be found in our revised manuscript.

**Text in manuscript**

**Abstract.**

...

Monthly NMVOC emissions over China in 2020 are then optimized by independently assimilating formaldehyde retrievals either from OMPS or from TROPOMI, using a self-developed ~~4DEnVar-based system. A positive increment of NMVOC emissions was obtained by assimilating OMPS formaldehyde , with annual anthropogenic emissions rising from 22.40 to 41.32 Tg, biogenic emissions increasing from 16.56 to 28.01 Tg, and biomass burning emissions rising from 0.29 to 0.65 Tg. Our model simulations, driven by the posterior inventories, demonstrate superior performance compared to the prior. This is validated through comparisons against the independent satellite measurements and the surface ozone measurements. The RMSE of the posterior formaldehyde columns decreased from 0.49 to 0.45 $\times 10^{16}$ molec/cm$^2$ nationwide. In the severe-polluted NCP, it was improved effectively, reaching levels comparable to TROPOMI~~ 4DEnVar assimilation emission inversion system.

...

**1 Introduction**

...

~~NMVOCs compared to OMI retrievals~~emission optimization at the national scale. Subsequently, the monthly NMVOC emission optimization in China is conducted. This is achieved by independently assimilating formaldehyde observations ~~from OMPS and~~ either from OMPS or from TROPOMI, based on the emission inversion system that couples the four-dimensional ensemble variational (4DEnVar) data assimilation algorithm and GEOS-Chem model. The effectiveness of this emission inversion system has been evaluated in our recent ~~study (Jin et al., 2023; Xia et al., 2025).~~ studies (Jin et al., 2023; Xia et al., 2025). In this study, we focus on the year 2020 for the main analysis, while results for 2019 are also presented in the Supplementary Information to provide additional context and support.

**RC:** ***2) Lack of Bias Correction for Satellite Data (Major) The study does not apply bias correction across satellite datasets, which is a critical omission. HCHO retrievals from OMPS and TROPOMI differ due to varying retrieval algorithms, cloud screening, and a priori assumptions. These systematic differences must be addressed before assimilation. Previous studies (e.g., Zhu et al., 2020; Müller et al., 2024) have shown the importance of bias correction using independent datasets such as aircraft or FTIR observations. At minimum, the authors should:***

- ***Justify the omission of bias correction***
- ***Discuss associated uncertainties***
- ***Provide quantitative comparisons between satellite datasets prior to assimilation (with figures in the main text)***
- ***Display and discuss the observation uncertainties used in the assimilation***

AR: We sincerely thank the reviewer for their valuable feedback on bias correction. In the revised manuscript, we have incorporated the following additions and clarifications:

Lack of independent observations for satellite data bias correction: Due to the unavailability of temporally coincident independent measurements (e.g., aircraft or FTIR data) over China in 2020, rigorous cross-satellite bias correction could not be performed. This limitation, as well as our mitigation approach, is now clearly acknowledged and discussed in the manuscript. To improve the comparability between OMPS and TROPOMI, we apply vertical profile corrections before the assimilation, including averaging kernel (AVK) adjustments for TROPOMI and air mass factor (AMF) recalculations for OMPS. In the assimilation, OMPS retrievals are used as total columns as provided by the product, while TROPOMI retrievals are assimilated as tropospheric columns. We did not construct total columns from TROPOMI, since doing so would introduce additional uncertainties. This choice does not affect comparability, because the model provides full vertical concentration profiles that can be integrated to both total and tropospheric columns, and formaldehyde is primarily distributed below the tropopause. These treatments make the assimilation more reliable.

Uncertainty discussion: We have expanded the Methods and Discussion sections to address observational uncertainties and their potential impacts on the assimilation results. Inter-satellite comparison: Prior to assimilation, we conducted a quantitative comparison of OMPS and TROPOMI retrievals, highlighting their differences relative to the prior. Both spatial and statistical comparisons are now included in the main text.

Presentation of observational uncertainties: Remarks concerning vertical profiles of observational uncertainties are now presented in the manuscript, with the Figures illustrating their spatial distributions provided in the Supplementary Material.

**Text Lack of independent observations for satellite data bias correction in manuscript**

**2.3.1 NOAA-20 OMPS**

...

Formaldehyde vertical column densities (VCDs) retrieved from satellite observations are derived using air mass factors (AMF), which strongly depend on the a priori vertical profiles of formaldehyde. Direct comparisons between satellite products and model simulations may be biased if the a priori profiles used in the retrieval differ from the simulated ones. To ensure consistency between the satellite observations and GEOS-Chem simulation, we applied an AMF correction by recalculating the AMF with model-simulated profiles following the method used in Palmer et al. (2001):

$$AMF = \int_{p_s}^{0} w\,(p) S\,(p)\,dp \tag{1}$$

...

The processed OMPS satellite observations were ultimately assimilated as total columns, which are presented in Figure 1 (c.1-c.4).

...

**2.3.2 Sentinel-5P TROPOMI**

...

Beyond the recommended quality screening, a key consideration when comparing TROPOMI formaldehyde

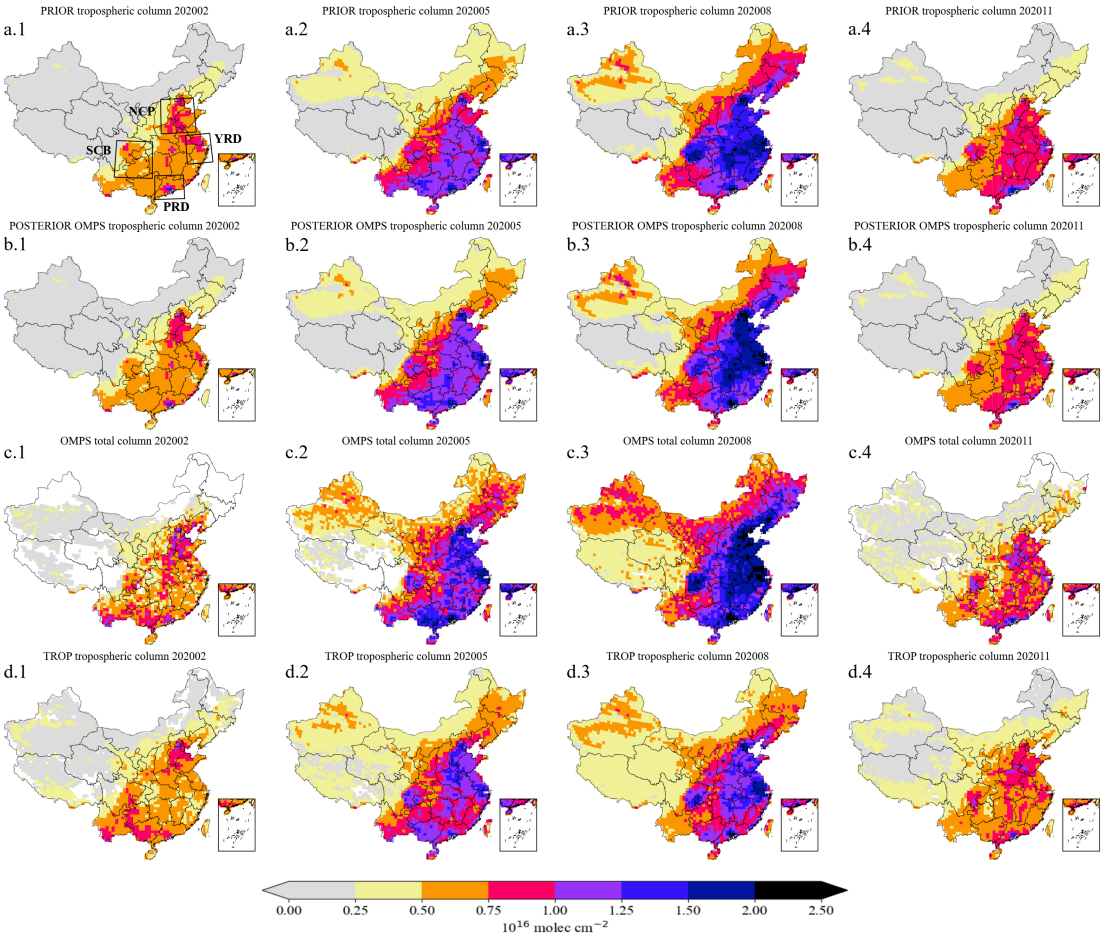


Figure 1. Spatial distributions of formaldehyde columns from GEOS-Chem model-simulated prior tropospheric columns (a) and posterior tropospheric columns constrained by OMPS assimilation (b), satellite observations of OMPS total columns (c), and satellite observations of TROPOMI tropospheric columns (d) in February (a.1-d.1), May (a.2-d.2), August (a.3-d.3), and November (a.4-d.4) of 2020.

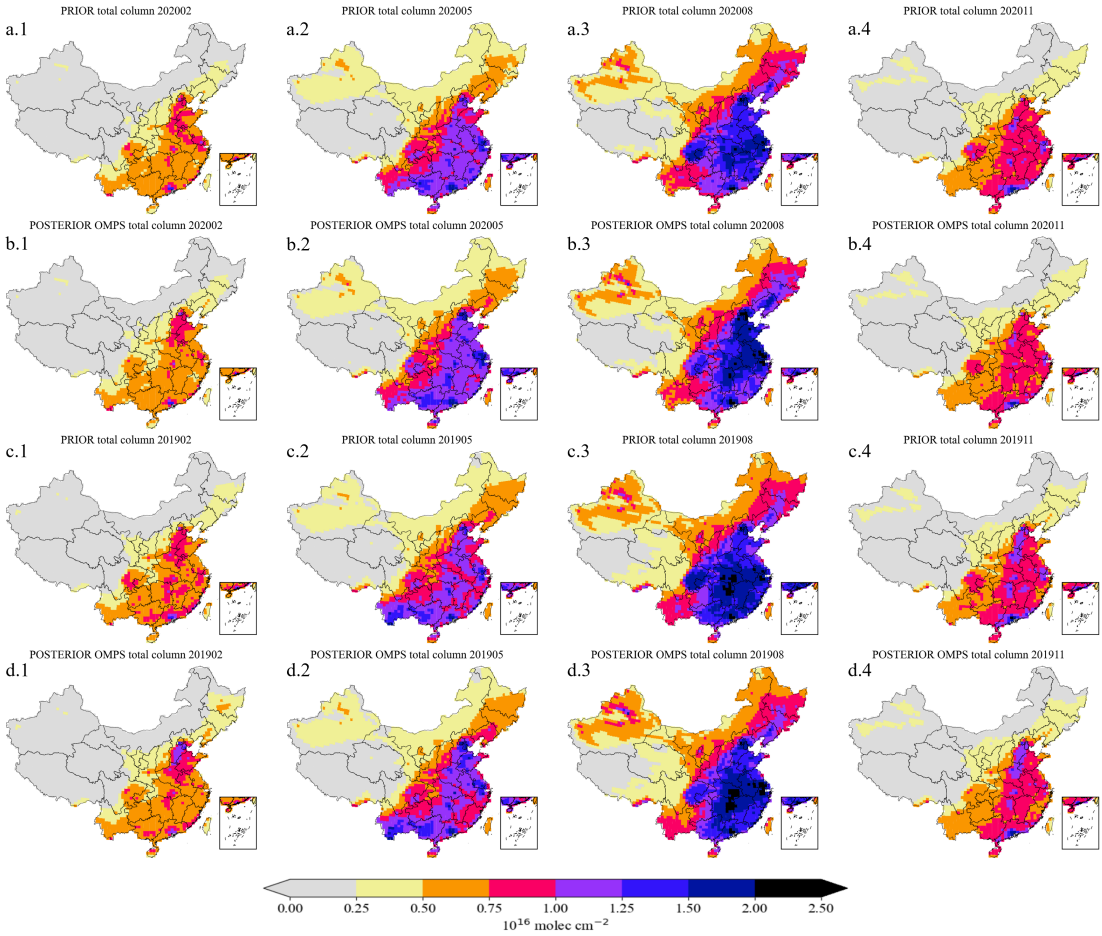


Figure 2. Spatial distributions of the formaldehyde total columns from GEOS-Chem model-simulated prior (a,c) and posterior (b,d) results in February (a.1-d.1), May (a.2-d.2), August (a.3-d.3), November (a.4-d.4) for 2020/2019.

retrievals with model outputs is the dependence on the assumed a priori vertical profile. Traditionally, studies have relied on AMF-based corrections, in which AMF is recalculated using model-derived profiles to reduce such discrepancies (Palmer et al., 2001; Boersma et al., 2004; Zhu et al., 2016; Cooper et al., 2020). More recently, the availability of averaging kernel (AVK) information in the TROPOMI product has allowed a more consistent comparison by accounting for the impact of the assumed vertical profile shape in the retrieval, following the approach introduced in the IASI $NH_3$ version 4 product (Clarisse et al., 2023; Xia et al., 2025). In this study, we apply AVK-based correction for TROPOMI formaldehyde by projecting the model profiles onto the satellite pressure grid, thereby achieving a more harmonized comparison with GEOS-Chem simulations. The corrected column is calculated as:

$$\hat{X}^m = \frac{\hat{X}^a - B}{\sum_p A_p^a m_p} + B \tag{2}$$

...

The processed TROPOMI retrievals were assimilated as tropospheric columns, which are presented in Figure 1 (d.1-d.4), with their vertical shape profiles shown in Figure 3 (green line) to illustrate the normalized contribution of each pressure layer to the tropospheric columns. We adopted tropospheric rather than total columns because the retrieval product itself provides tropospheric columns, and recalculating total columns would introduce substantial uncertainties.

...

**2.3.3 Aura OMI**

The OMI observations are then aggregated to monthly means on a $0.5° \times 0.625°$ grid, consistent with the GEOS-Chem model resolution. To ensure sufficient sampling per grid cell, we also applied two filtering schemes based on the number of observations, excluding grid cells with fewer than 10 or fewer than 50 valid pixels. Unlike OMPS and TROPOMI, however, OMI shows a strong reduction in data coverage under these constraints, and the product becomes sparse after applying the threshold of 50 observations. This indicates that OMI suffers from insufficient sampling density in China for high-resolution assimilation. The vertical profile correction of OMI formaldehyde was conducted using the same approach as applied to OMPS, by recalculating AMF with model-simulated vertical profiles.

...

**4 Summary and conclusion**

...

Future efforts should reassess assimilation performance with updated emission inventories and incorporate source-specific uncertainties, assigning different uncertainties to anthropogenic, biogenic, and biomass burning sectors, in order to better constrain their respective emissions. Moreover, because no independent validation data such as aircraft or FTIR measurements were available over China in 2020, future studies could further evaluate the assimilation results once such observational datasets become accessible.

**Text Uncertainty discussion and Presentation of observational uncertainties in manuscript**

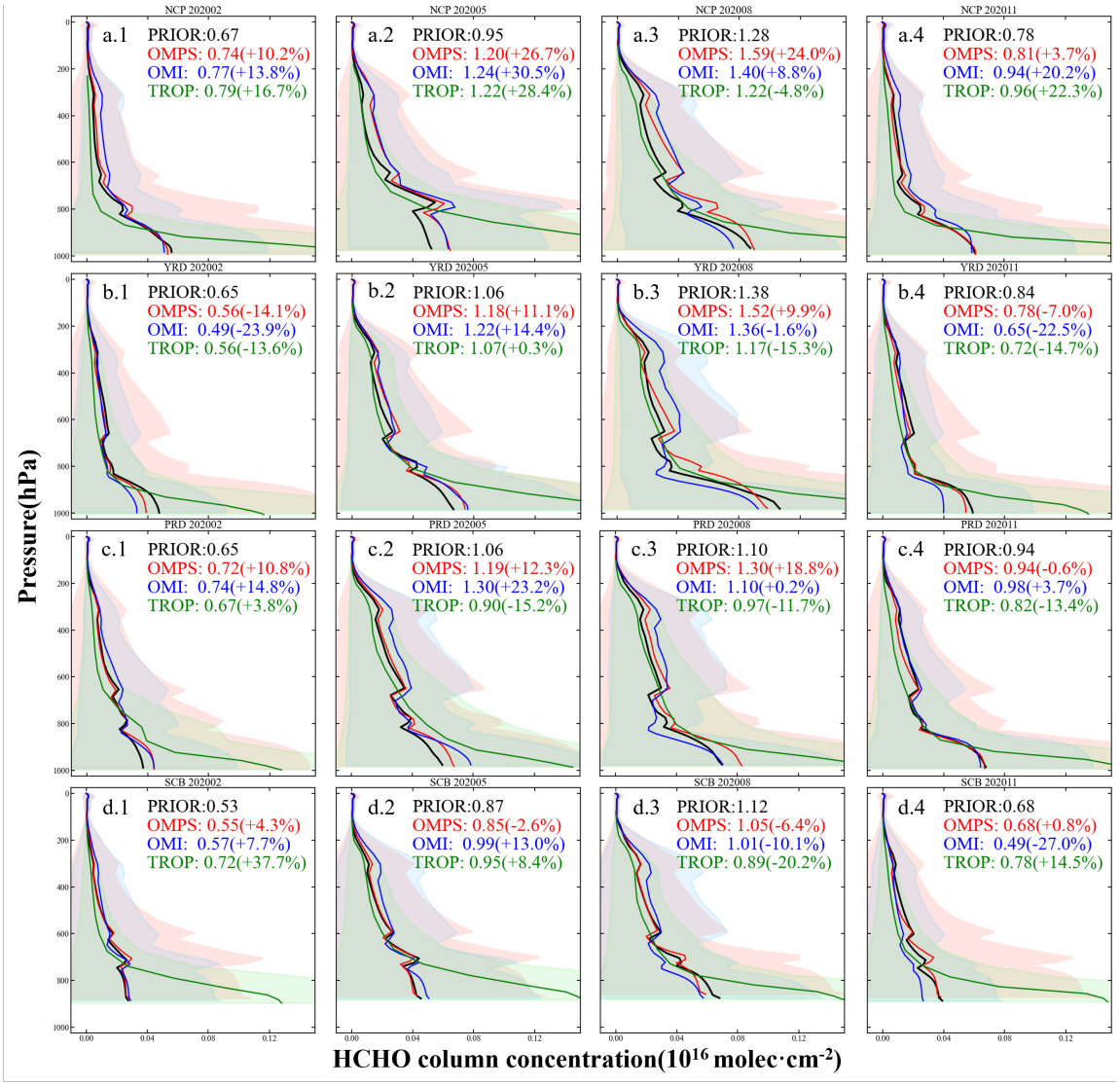


Figure 3. Vertical distributions of the regional mean formaldehyde columns from GEOS-Chem model-simulated prior (black) and satellite observations by OMPS (blue), TROPOMI (red), and OMI (green). Panels (a)-(d) correspond to the North China Plain, Yangtze River Delta, Pearl River Delta, and Northeast China, respectively. Sub-panels (a.1-d.1), (a.2-d.2), (a.3-d.3), and (a.4-d.4) represent February, May, August, and November 2020, respectively. Values in parentheses indicate the biases of satellite observations relative to the prior simulation. Shaded areas denote the observational uncertainties.

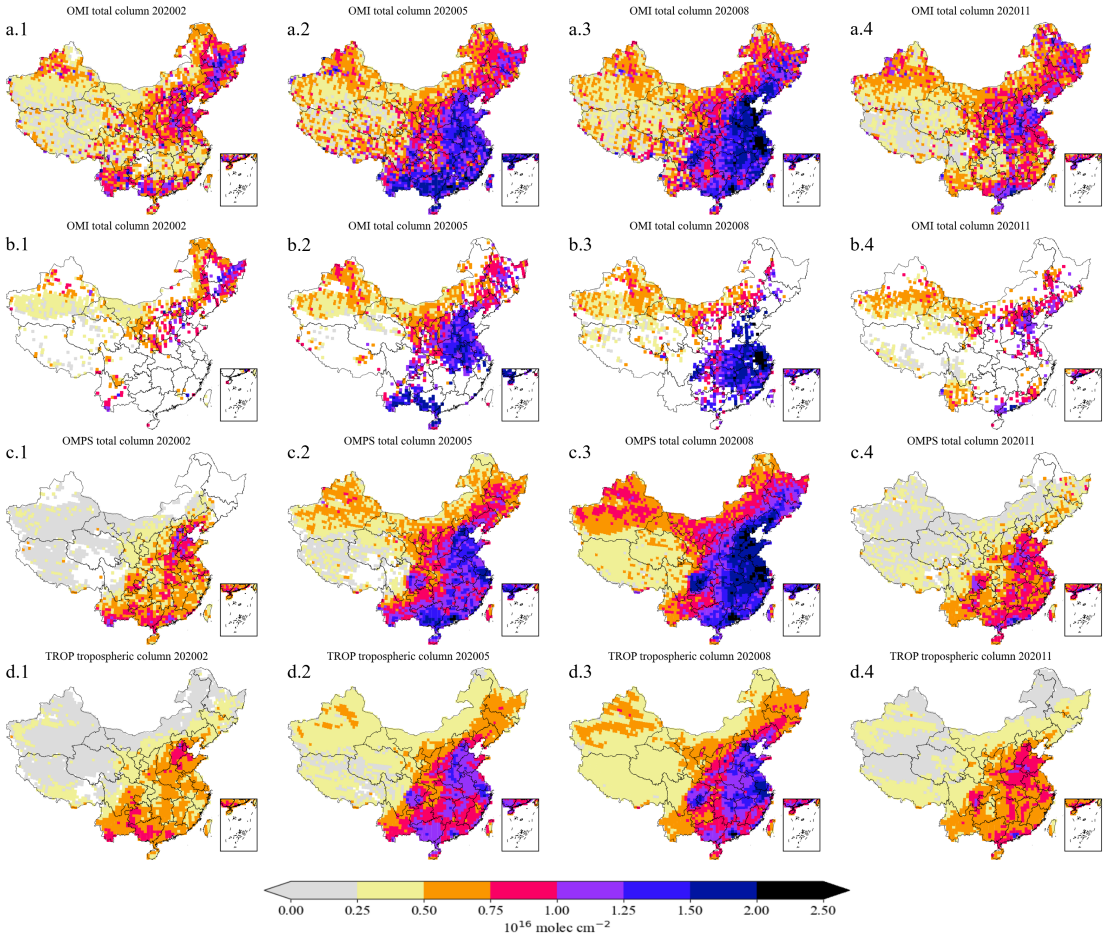


Figure 4. Comparison of monthly mean formaldehyde column concentrations in February, May, August, and November 2020 after applying different data filtering thresholds. Panels (a.1-a.4), (c.1-c.4), and (d.1-d.4) show OMI, OMPS, and TROPOMI results, respectively, after removing grid cells with fewer than 10 observations. Panels (b.1-b.4) show OMI results after removing grid cells with fewer than 50 observations.

~~3.1 Semi-variogram analysis~~**3.1 Satellite data evaluation**

...

Uncertainty is a key component in the assimilation process and serves as a crucial indicator of satellite data quality. Figure 3 illustrates the vertical distribution of retrieval uncertainties. In the mid- to upper troposphere (200-600 hPa), OMPS and OMI show comparable levels of uncertainty. However, below 600 hPa, OMPS uncertainties become substantially larger, likely due to cloud contamination and retrieval algorithm approximations (González Abad et al., 2016; Nowlan et al., 2023). As shown in ~~the four interpolated results in Figure 3, the spatial distribution of high formaldehyde values is consistently captured across different horizontal resolutions, either by the satellite observations in Figure 3~~Supplementary Figure **??**, the overall uncertainty of OMPS is significantly higher than that of the other two satellite datasets. At first glance, OMI data may appear superior, but this advantage largely results from strict filtering, which excludes a substantial fraction of problematic data. As illustrated in Supplementary Figure 4 (a, b~~, c)or by GEOS-Chem simulation in panel (d). These hot spots are particularly prominent in the North China Plain (NCP) and Jiangsu-Zhejiang-Shanghai regions. However, at the higher resolution of 0.5° x 0.5°, OMI formaldehyde data exhibits noticeable noise all over China and lacks the spatial continuity observed in TROPOMI, OMPS, and GEOS-Chem datasets. The significant spatial variability in the NMVOC emission field might account for the discontinuity observed in OMI formaldehyde data . However, this discontinuity contradicts the model simulation and the other two satellite products obtained from the more advanced instruments. Moreover, such discontinuities are not observedin OMI formaldehyde retrievals over the United States, where (Kaiser et al., 2018) demonstrated continuous and high-quality data. Therefore, the discrepancies observed in China may be attributed to uncertain input parameters, such as aerosols and surface albedo. OMI formaldehyde retrievals with larger spatial grid intervals (2° x 2° ), applying a threshold of 50 observations per grid cell drastically reduces spatial coverage, rendering OMI unsuitable for national-scale assimilation. Previous studies that assimilated OMI over China have typically interpolated the data to coarser resolutions to ensure applicability (Cao et al., 2018; Miyazaki et al., 2020). Therefore, only OMPS and 4° x 4°) exhibit increased continuity and smoothness, as shown in Figure 3(a). This improvement is attributed to spatial averaging, which effectively filters out white noise (Lee, 1980).~~

**Text Inter-satellite comparison in manuscript**

**3.1 Satellite data evaluation**

...

Figure 3 also presents satellite retrieval deviations from the prior model estimates. When all three satellite datasets exhibit the same sign of deviation (positive or negative) relative to the model, they are considered consistent. Such consistency is observed, for example, in February, May, and November over NCP and in February over PRD and SCB, where all three datasets show positive deviations; and in February and November over YRD and in August over SCB, where all show negative deviations. These cases indicate stronger reliability. In other situations, when OMPS and TROPOMI exhibit the same bias direction, they are also considered consistent, as in November over PRD and SCB. Overall, ~~at higher spatial resolutions, OMI formaldehyde data exhibit more white noise, with higher semi-variance values and weaker spatial autocorrelation.~~

...

### 3.3 Formaldehyde ~~total~~ columns evaluation

The spatial distributions of formaldehyde columns in February, May, August, and November 2020 are shown in Figure ~~1 (a) and (b), GEOS-Chem simulated the prior and posterior estimates of formaldehyde for four months of the year 2020 over China. In Figure 1 (a) , the prior results exhibit a spatial distribution similar to satellite observations . When compared to OMPS and~~ 1. Panels (a.1-a.4) display the prior simulations of tropospheric columns, (b.1-b.4) present the posterior simulations of tropospheric columns assimilated by OMPS, (c.1-c.4) show the OMPS satellite observations of total columns, and (d.1-d.4) illustrate the TROPOMI satellite observations of tropospheric columns. In addition, the prior ~~results accurately reproduce high-value features in most regions, including Yunnan-Guizhou, Guangxi-Guangdong, NCP, the southeastern coast, and the northeast. However, the previous simulation did not accurately represent the actual formaldehyde levels. Specifically, it underestimated formaldehyde concentrations to varying degrees across different regions. By assimilating OMPS formaldehyde columns, improvement was obtained steadily in the posterior simulations. Nationwide, the posterior formaldehyde columns were raised by approximately 50%. Comparing to TROPOMI data used as independent measurements, the~~ and posterior simulations of total columns for 2020 are also provided in the Supplementary Figure 2. As indicated by the vertical profiles in Figure 3, formaldehyde ~~levels~~ is mainly distributed below the tropopause. Comparisons between the prior and posterior results show that the differences between total and tropospheric columns are relatively small. Regarding the spatial patterns, high formaldehyde values in February are concentrated in the NCP~~region were raised from less than 1.2 $\times 10^{16}$ molec/cm$^2$ to around 2.4 $\times 10^{16}$ molec/cm$^2$ in January, closer to the observed values either from OMPS and TROPOMI. The~~ , YRD, and PRD regions, with the posterior results showing an expanded high-value ~~features in Yunnan-Guizhou became more prominent in April, and significant improvements were also observed in the southeastern coast, NCP, and the northeast in July and October. However,~~ area in the NCP but a reduced coverage in the YRD. In May, overall concentrations increase nationwide, with particularly pronounced growth in the NCP and PRD. In August, concentrations increase in the NCP, YRD, and PRD, while they decrease in the SCB. In November, the changes are modest, but all four regions exhibit reduced concentrations.

**RC:** ***3) Unrealistic Assumptions for Emission Uncertainty (Major) The manuscript assumes a uniform 100% random uncertainty for all emission sectors and species. This is overly simplistic and not representative of known variability-biogenic and biomass burning emissions typically carry much greater uncertainty than anthropogenic sources. Furthermore, the spatial correlation structure of errors and the regularization approach are not well described. These assumptions critically affect the inversion and should be better supported by literature references, sensitivity tests, or at minimum, a comprehensive uncertainty discussion.***

AR: We thank the reviewer for this important comment. For testing the uncertainty choice, we adopted sector-specific prior uncertainties of 150% for anthropogenic VOCs, 200% for biogenic VOCs, and 300% for biomass burning VOCs (following Souri et al. (2020)). These were combined using a weighted quadratic formulation, which yielded a total uncertainty of about 120%. Accordingly, we set the standard deviation of the multiplicative factor to 0.4. To test the simplification of applying a uniform total uncertainty, we compared emissions based on sector-weighted uncertainties with those obtained by uniformly scaling the prior by 120% (Figure 5), and found the two distributions to be generally consistent. This supports the reasonableness of our assumption, while we acknowledge that uniform uncertainties remain a simplification, and sector-specific inversions will be explored in future work. Remarks concerning the spatial correlation structure in the background error covariance have also been added in the revised manuscript.

**Text in manuscript**

Table 1. Uncertainty assumptions for different emission sectors.

| | Anthropogenic | Biogenic | Biomass burning |
|---|---|---|---|
| VOC | 150% | 200% | 300% |

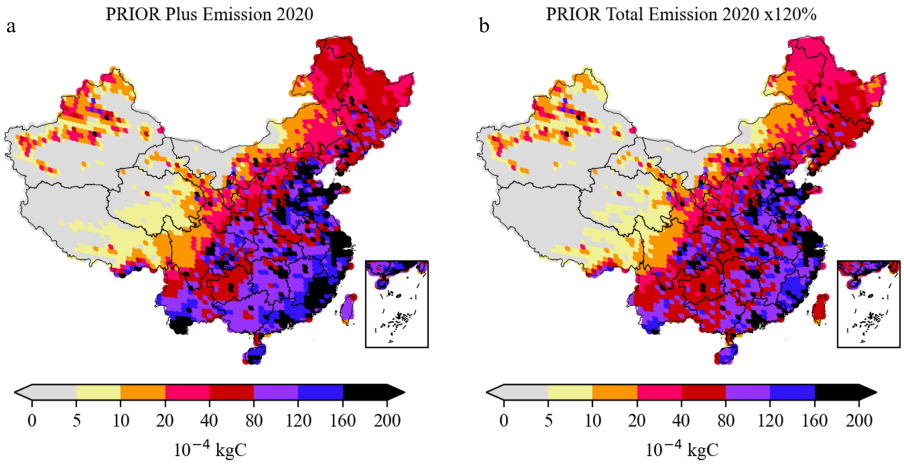


Figure 5. Comparison of prior NMVOC emissions estimated by combining sector-specific uncertainties (a) and by uniformly scaling the prior total emissions by 120% (b) in 2020. The two distributions are generally consistent, supporting the applicability of the total uncertainty assumption used in this study.

**2.5 Assimilation algorithm**

...

The uncertainty in the NMVOCs simulation is assumed to be attributed to errors in the emission inventories, and can be compensated using a spatially varying tuning factor $\alpha$:

$$f(i) = f_b(i) \cdot \alpha(i) \tag{3}$$

in here $f_b(i)$ denotes the NMVOC emission rate in the given grid cell $i$. The $\alpha$ values are defined to be random variables with a mean of 1.0, a minimum of 0.1 and a standard deviation ~~$\sigma_\alpha = 0.2$~~of 0.4, corresponding to a uniform 120% uncertainty applied to the total NMVOC emissions rather than sector-specific settings as adopted in previous studies (Choi et al., 2022; Jung et al., 2022; Souri et al., 2020) . The rationale for this choice is provided in the Supplement. This empirical value was found to provide sufficient spaces for resolving the observation-minus-simulation errors. A background covariance $\mathbf{B}_\alpha$

is formulated as a product of the constant standard deviation and a spatial correlation matrix $\mathbf{C}$:

$$\mathbf{B}_\alpha(i,j) = \sigma_\alpha \cdot \mathbf{C}(i,j) \tag{4}$$

where $\mathbf{C}(i,j)$ represents a distance-based spatial correlation between two $\alpha$s in the grid cell $i$ and $j$, and is defined as:

$$\mathbf{C}(i,j) = e^{-(d_{i,j}/l)^2/2} \tag{5}$$

where $d_{i,j}$ represents the distance between two grid cells $i$ and $j$. $l$ here denotes the correlation length scale which controls the spatially variability freedom of the $\alpha$s. A small value of $l$ ~~means more errors in fine scale could be resolved using the assimilation, while however requires more~~ indicates that the tuning factors $\alpha$s are less spatially correlated, thereby enabling emission optimization at a finer spatial scale. However, this also necessitates a larger number of ensemble runs to adequately represent the model realization from emission to simulation. An empirical ~~parameterl~~ parameter $l$ = 300 km which is used in Jin et al. (2023) to nudge the ammonia emission that has a rapid spatially variability is also taken in this study. With the covariance matrix $\mathbf{B}_\alpha$, the NMVOC emission background covariance $\mathbf{B}$ is obtained via a Schur Product:

$$\mathbf{B} = \mathbf{B}_\alpha \circ \mathbf{C} \tag{6}$$

...

**Supplement**

**1 Emission Uncertainty**

Following previous studies (Souri et al., 2020), sector-specific prior uncertainties for anthropogenic, biogenic, and biomass burning emissions can be combined into a total uncertainty using a weighted approach.

$$\sigma^2_{\text{total}} = f^2_{\text{anthro}} \cdot \sigma^2_{\text{anthro}} + f^2_{\text{biogenic}} \cdot \sigma^2_{\text{biogenic}} + f^2_{\text{bioburn}} \cdot \sigma^2_{\text{bioburn}} \tag{7}$$

Applying this method to the uncertainty values reported in earlier work, we obtained a total prior uncertainty of 120.22%. Accordingly, we set the standard deviation of the multiplicative factor to 0.4 in this study. To assess the validity of this simplification, we compared the sector-weighted prior emissions (Figure 5 (a)) with the prior emissions uniformly scaled by 120% (Figure 5 (b)). The two results are generally consistent, supporting the reasonableness of adopting a uniform total uncertainty in this study. Sector-specific inversion will be considered in future work.

**RC:** ***4) Inversion Framework and Terminology (Major) The manuscript describes the method as 4DEnVar, yet***

***no ensemble component appears to be used. The inversion resembles a standard 4D-Var framework. If an ensemble is not implemented, the use of "EnVar" terminology is misleading and should be corrected. If an ensemble is used, key details are missing, including ensemble generation, localization, hybrid covariance structures, etc. Additionally, the manuscript does not explain:***

- ***The optimization method used to minimize the cost function***
- ***Convergence criteria and number of iterations***
- ***Use and selection of regularization***
- ***Whether the GEOS-Chem adjoint model is used, and how it is implemented***

AR: We agree with the referee that the more details concerning the 4DEnVar should be given. The methodology used in this paper is actually 4DEnVar, which emulates the GEOS-Chem formaldehyde simulating model using an ensemble-based linear approximation and hence is adjoint-free. More remarks are now added in the revised manuscript and the supplement.

**Text in manuscript**

**2.5 Assimilation algorithm**

This study employs the four-dimensional ensemble variational (4DEnVar) methodology to ~~assimilate formaldehyde observations to constrain NMVOC emissions~~ optimize NMVOC emissions with satellite formaldehyde observations. The goal of ~~this~~ the assimilation is to find the most likely estimate of the state vector, which is the monthly NMVOC emission inventories $\boldsymbol{f}$ over the entire model domain. Note that $\boldsymbol{f}$ represents the vector of total NMVOC emissions, rather than separately gridded anthropogenic, biogenic, or biomass burning VOC emissions. To optimize emissions from these three sectors, additional observations or a well-defined spatial correlation structure are required, which are not available in this study. The prior estimate $\boldsymbol{f}_b$ is from the inventories described in Section 2.2, and the formaldehyde concentration observations $\boldsymbol{y}$ are described in Section 2.3. Mathematically, assimilation is performed via minimizing the cost function $J$ as follows:

$$\mathcal{J}(\boldsymbol{f}) = \frac{1}{2}(\boldsymbol{f}-\boldsymbol{f}_b)^T\mathbf{B}^{-1}(\boldsymbol{f}-\boldsymbol{f}_b) + \frac{1}{2}\left\{\boldsymbol{y}-\mathcal{HM}\left(\boldsymbol{f}\right)\right\}^T\mathbf{O}^{-1}\left\{\boldsymbol{y}-\mathcal{HM}\left(\boldsymbol{f}\right)\right\} \tag{8}$$

The cost function $\mathcal{J}$ is the sum of two ~~part~~parts: background and observation penal term. The background term quantifies the difference between the optimal $\vec{f}$ and the prior emission inventories $\vec{f_b}$, while the observation term calculates the difference between the simulation driven by $\vec{f}$ and the satellite observations $\vec{y}$. In addition to the $\boldsymbol{f}_b$ that represents the prior NMVOC emission vector calculated from the anthropogenic, biogenic, and biomass burning sources as been illustrated in Section 2.2. The uncertainty in the NMVOCs simulation is assumed to be attributed to errors in the emission inventories, and can be compensated using a spatially varying tuning factor $\alpha$:

$$f\left(i\right) = f_b\left(i\right)\cdot\alpha\left(i\right) \tag{9}$$

in here $f_b(i)$ denotes the NMVOC emission rate in the given grid cell $i$. The $\alpha$ values are defined to be random variables with a mean of 1.0, a minimum of 0.1 and a standard deviation ~~$\sigma_\alpha = 0.2$~~of 0.4, corresponding to a uniform 120% uncertainty applied to the total NMVOC emissions rather than sector-specific settings as adopted in previous studies (Choi et al., 2022; Jung et al., 2022; Souri et al., 2020) . The rationale for this choice is provided in the Supplement. This empirical value was found to provide sufficient spaces for resolving the observation-minus-simulation errors. A background covariance $\mathbf{B}_\alpha$ is formulated as a product of the constant standard deviation and a spatial correlation matrix $\mathbf{C}$:

$$\mathbf{B}_\alpha(i,j) = \sigma_\alpha \cdot \mathbf{C}(i,j) \tag{10}$$

where $\mathbf{C}(i,j)$ represents a distance-based spatial correlation between two $\alpha$s in the grid cell $i$ and $j$, and is defined as:

$$\mathbf{C}(i,j) = e^{-(d_{i,j}/l)^2/2} \tag{11}$$

where $d_{i,j}$ represents the distance between two grid cells $i$ and $j$. $l$ here denotes the correlation length scale which controls the spatially variability freedom of the $\alpha$s. A small value of $l$ ~~means more errors in fine scale could be resolved using the assimilation, while however requires more~~ indicates that the tuning factors $\alpha$s are less spatially correlated, thereby enabling emission optimization at a finer spatial scale. However, this also necessitates a larger number of ensemble runs to adequately represent the model realization from emission to simulation. An empirical ~~parameterl~~ parameter $l$ = 300 km which is used in Jin et al. (2023) to nudge the ammonia emission that has a rapid spatially variability is also taken in this study. With the covariance matrix $\mathbf{B}_\alpha$, the NMVOC emission background covariance $\mathbf{B}$ is obtained via a Schur Product:

$$\mathbf{B} = \mathbf{B}_\alpha \circ \mathbf{C} \tag{12}$$

In the observation term, $\boldsymbol{y}$ is the observation vector, representing satellite observations, $\mathcal{M}$ is the GEOS-Chem model driven by emissions $\boldsymbol{f}$, $\mathcal{H}$ is the observation operator that ~~transfer the three dimensional~~ transfers the three-dimensional concentration into the observational space, and $\mathbf{O}$ is the observation covariance matrix. In this study, the assimilated observations include the OMPS total columns and TROPOMI tropospheric columns. A distinct observation operator $\mathcal{H}$ is configured to enable a fair comparison of the observation-minus-simulation mismatch. The satellite formaldehyde observations are assumed to be independent, therefore $\mathbf{O}$ is a diagonal matrix. The diagonal value here is calculated as:

$$\sigma_{\text{total}} = \sqrt{\sigma^2_{\text{instrument}} + \sigma^2_{\text{represent}}} \tag{13}$$

In ~~the~~ Equation 34, $\sigma_{\text{total}}$ is defined as the total uncertainty, which is the square root of the sum of the squares of the instrument uncertainty $\sigma_{\text{instrument}}$ from the formaldehyde observations and the representative uncertainty $\sigma_{\text{represent}}$ introduced when processing the data into monthly averages. The representative uncertainty $\sigma_{\text{represent}}$ is represented by the standard deviation of the data.

~~With the assimilation-based emission inversion system above, we conducted three sets of experiments to explore the benefits to emission optimization. These experiments involved assimilating OMPS data and validating the assimilation results using TROPOMI, assimilating TROPOMI data, and finally assimilating the combined OMPS and TROPOMI data by averaging them. In the subsequent results, we primarily analyze the results of the first set of experiments, while the detailed inventories of the latter two experiments are archived in~~ The spatial distribution of the total uncertainty is provided in Figure 4 in the Supplement.

The assimilation methodology used in this paper is the four-dimensional ensemble variational (4DEnVar). Different from the classic 4DVar that requires adjoint in the cost function minimization, 4DEnVar emulates the GEOS-Chem formaldehyde simulating model using an ensemble-based linear approximation and hence is adjoint-free. The method is first proposed by Liu et al. (2008) and successfully implemented in our recent dust aerosol (Jin et al., 2021) and ammonia emission inversion (Jin et al., 2023; Xia et al., 2025) . The detailed procedures for minimizing the cost function Equation 29 are illustrated in section 'Minimization of the Cost Function in 4DEnVar' in supplementary material.

**Supplement**

## 2 Minimization of the Cost Function in 4DEnVar

The minimization of the cost function follows the 4DEnVar processes. An ensemble of emission inventory is generated randomly using the prior emission vector $f$ and the assumed emission error covariance $\mathbf{B}$:

$$[f_1, \ldots, f_N] \tag{14}$$

An ensemble of GEOS-Chem model simulations is then forward run with the ensemble emission inventories in parallel:

$$[\mathcal{M}(f_1), \ldots, \mathcal{M}(f_N)] \tag{15}$$

Denote the emission ensemble perturbation matrix by:

$$F' = \frac{1}{\sqrt{N-1}}[f_1 - \bar{f}, \ldots, f_N - \bar{f}] \tag{16}$$

and the mean of ensemble simulation by:

$$\mathcal{M}(\bar{f}) = \frac{1}{N}\sum_{i=1}^{N}\mathcal{M}(f_i) \tag{17}$$

where $\bar{f}$ is the mean of the ensemble emission inventories. In the 4DEnVar assimilation algorithm, the optimal emission $f$ is defined as a weighted sum of the columns of the perturbation matrix $F'$ using weights from a control variable vector $w$:

$$f = \bar{f} + F'w \tag{18}$$

The cost function could then be reformulated as:

$$\mathcal{J}(w) = \frac{1}{2}w^T w + \frac{1}{2}\left\{H\mathcal{M}'w + H\mathcal{M}(\bar{f}) - y\right\}^T \mathbf{O}^{-1}\left\{H\mathcal{M}'w + H\mathcal{M}(\bar{f}) - y\right\} \tag{19}$$

where $\mathcal{M}$ is the linearization of the GEOS-Chem formaldehyde simulating model required for cost function minimization, and is approximated by:

$$\mathcal{M}'F' \approx \frac{1}{\sqrt{N}}\left[\mathcal{M}(f_1) - \mathcal{M}(\bar{f}), \ldots, \mathcal{M}(f_N) - \mathcal{M}(\bar{f})\right] \tag{20}$$

With the uncertainty in emission transferred into the observation space, the minimum of the cost function in Equation 40 could then be directly calculated, and the posterior emission $f$ subsequently updated.

$$m_z = \frac{M_z^m - B_z}{M^m - B} \tag{21}$$

Here $M_z^m$ represents the modeled concentration of formaldehyde at altitude $z$, $B_z$ is the background concentration of formaldehyde at the same altitude, $M^m$ represents the total modeled concentration

of formaldehyde in the atmosphere, and $B$ is the total background concentration.

$$A_z^a = \frac{1}{N}\frac{\hat{X}^a - B}{\hat{X}^l - B} \tag{22}$$

Here $X_z^a$ represents the a priori (or assumed) concentration of formaldehyde at altitude $z$, $B_z$ is again the background concentration at the same altitude, $\hat{X}^a$ is the total a priori concentration, and $N$ is a normalization factor ensuring the matrix $A_z^a$ sums correctly to account for all altitudes.

**RC:** ***5) Incomplete Statistical Evaluation of Results (Major) The validation of the inversion results relies solely on RMSE. A more complete suite of statistical metrics is needed, including correlation coefficient, bias, normalized mean bias (NMB), and potentially others. This will allow for a more comprehensive understanding of model performance and assimilation impact.***

AR: Thank you for this helpful comment. We agree that RMSE alone is insufficient for a comprehensive evaluation. In the revised manuscript, we have added additional statistical metrics, including correlation coefficient (R), coefficient of determination ($R^2$), mean absolute error (MAE), regression slope, and intercept, in addition to RMSE. As shown in Figure 6, these metrics consistently demonstrate improved agreement of the posterior simulations with TROPOMI across China and in key regions (NCP, YRD, PRD, SCB). This provides a more complete and robust assessment of the assimilation impact.

**Text in manuscript**

3.3 Formaldehyde ~~total~~ columns evaluation

...

The prior and OMPS-driven posterior simulations of formaldehyde tropospheric columns were compared with the TROPOMI formaldehyde tropospheric columns to evaluate the changes in ~~Inner Mongolia, Tibet, and the northwest were minimal. This is because the assigned background uncertainty, which is proportional to~~ formaldehyde. Scatter plots together with statistical metrics ($R^2$, R, MAE, and RMSE) for the ~~prior emission intensity in these regions, was particularly low, leaving limited flexibility for adjustments in the assimilation. This can be best seen in Figure 2, these areas are depicted in gray on the map, with annual total emissions below $5 \times 10^{-4} kg/m^2$, and the actual values for some grid points in these regions are even less than~~ whole country and four subregions in 2020 are presented in Figure 6. The prior simulation already shows reasonably good performance (a.1-e.1), with most points distributed close to the 1$~~\times 10^{-4} kg/m^2$. Though assimilating OMPS observations:~~1 line and exhibiting strong correlations with observations. Nevertheless, further improvements are still possible. After assimilating OMPS data, the posterior ~~simulation in these regionsstill remains low, resulting in little change. As illustrated in Figure 7 (a.2, a.3)~~results compared with TROPOMI show higher $R^2$ values across all regions, ~~the minimal changes in these areas also affected the national observation-minus-simulation discrepancies (root mean square error , RMSE), which decreased from $0.49 \times 10^{16}$ molec/cm$^2$~~ indicating strengthened correlations. For China and NCP, the improvements are comparable, with $R^2$ increasing by about 0.027 (from 0.870 to ~~$0.46 \times 10^{16}$ molec/cm$^2$. However,~~

~~as shown in Figure 7 (b.2) -(b.3) , when focused on the NCP region, the RMSE decreased from 0.53 $\times 10^{16}$ molec/cm$^2$~~ 0.897 for China, and from 0.774 to ~~0.37 $\times 10^{16}$ molec/cm$^2$effectively.~~

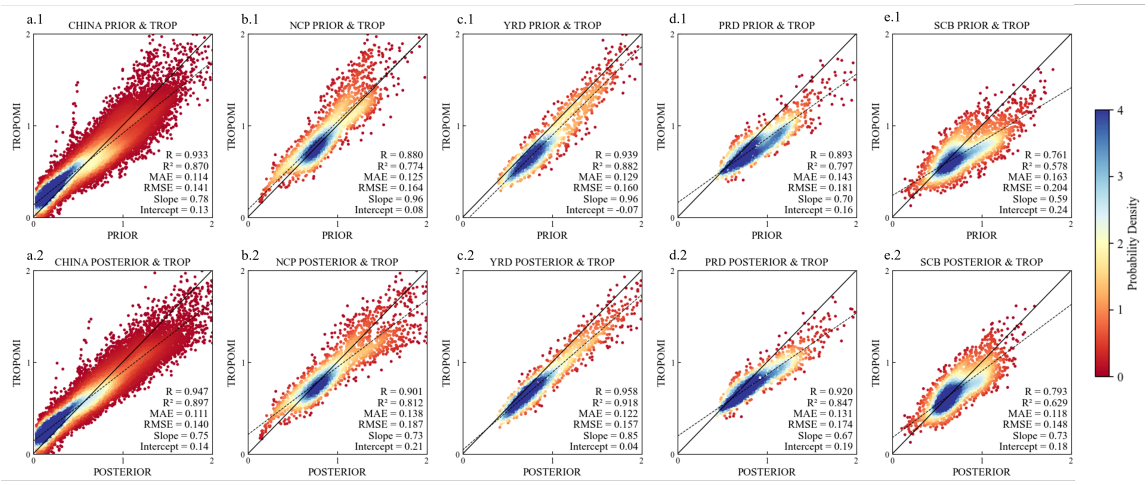


Figure 6. Scatter density plots comparing GEOS-Chem simulated formaldehyde columns with TROPOMI observations in 2020. Panels (a.1-e.1) show comparisons between prior simulations and TROPOMI, while panels (a.2-e.2) show comparisons between posterior simulations constrained by assimilating OMPS observations and TROPOMI. The regions considered are China (a), the North China Plain (b), the Yangtze River Delta (c), the Pearl River Delta (d), and the Sichuan Basin (e). The probability density of the data points is indicated by the color scale. The correlation coefficient (R), coefficient of determination ($R^2$), mean absolute error (MAE), root mean square error (RMSE), regression slope, and intercept are reported in each panel.

**RC:** ***6) Insufficient Discussion of Scientific Implications (Major) The target year, 2020, was heavily influenced by COVID-19-related emission reductions. This critical context is not introduced in the manuscript and must be incorporated into both the introduction and discussion sections. Specifically:***

- ***Why was 2020 chosen for the inversion?***
- ***How do inversion results indicating underestimation in prior emissions reconcile with pandemic-related expectations of reduced emissions?***
- ***What implications do the findings have for air quality modeling or emission policy evaluation?***

AR: We sincerely thank the reviewer for highlighting the importance of contextualizing our study with respect to COVID-19-related emission reductions. Although 2020 was indeed influenced by COVID-19, this was not the primary reason for selecting it as the study year. To avoid potential biases arising from a single anomalous year, we additionally conducted assimilation experiments for 2019 as a comparison. The results show that formaldehyde concentrations in 2019 were generally higher than in 2020, but in both years the prior consistently underestimated the observations to some extent. Assimilation substantially improved the simulation of both formaldehyde and ozone across multiple regions and seasons. For example, notable consistency enhancements and RMSE reductions were observed over the North China Plain in June, the

Yangtze River Delta in February and October, the Pearl River Delta in January, February, June, and July, and the Sichuan Basin in January, February, June, July, and September-December (Figure 8). These findings indicate that the prior underestimation cannot be fully attributed to pandemic-related emission changes, but rather reflects intrinsic uncertainties in the bottom-up emission inventories.

**Text in manuscript**

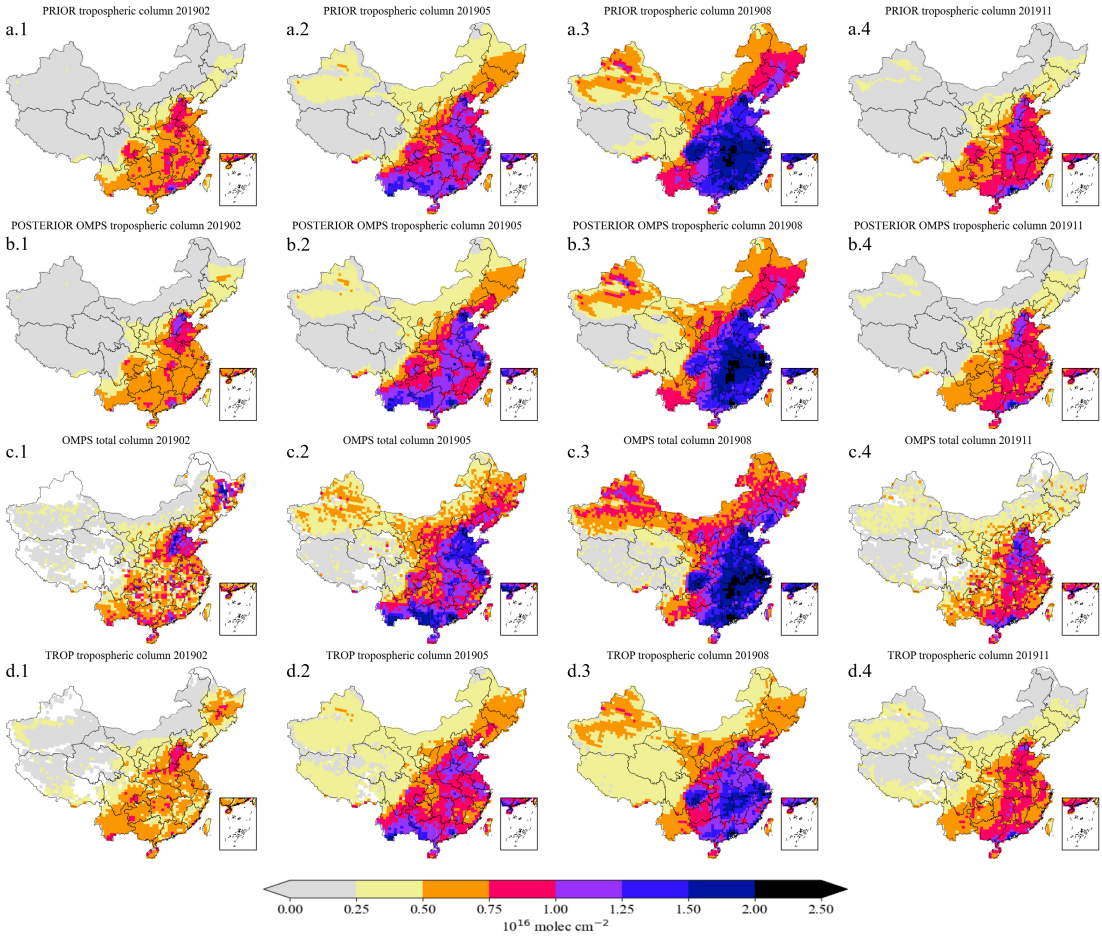


Figure 7. Spatial distributions of formaldehyde columns from GEOS-Chem model-simulated prior tropospheric columns (a) and posterior tropospheric columns constrained by OMPS assimilation (b), satellite observations of OMPS total columns (c), and satellite observations of TROPOMI tropospheric columns (d) in February (a.1-d.1), May (a.2-d.2), August (a.3-d.3), and November (a.4-d.4) of 2019.

**1 Introduction**

...

In this study, we focus on the year 2020 for the main analysis, while results for 2019 are also presented

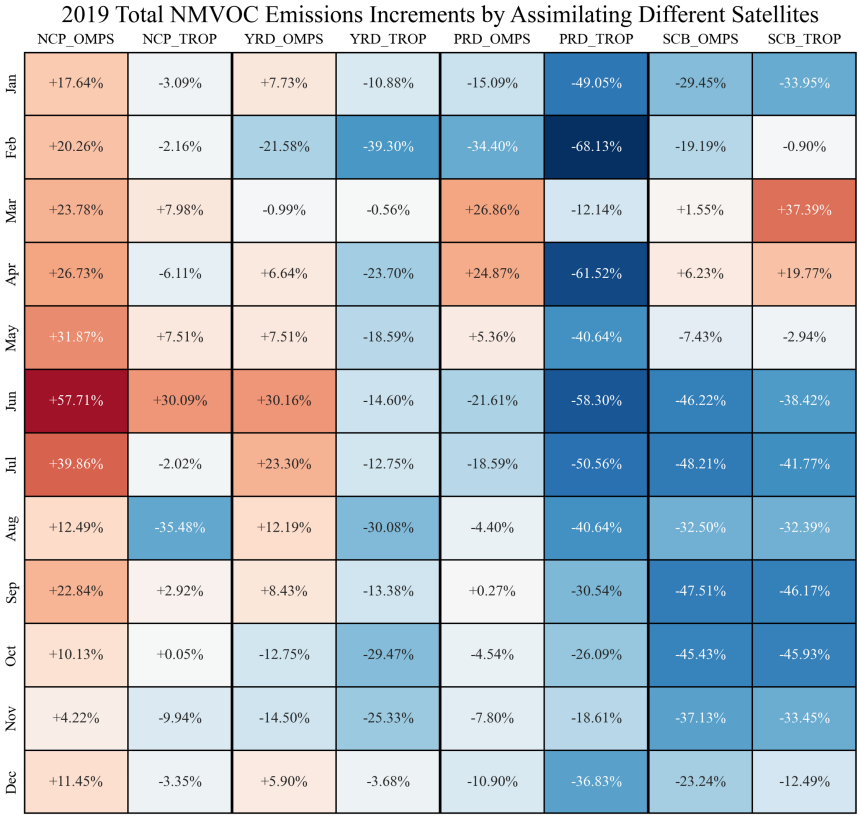


Figure 8. Monthly increments in total NMVOC emissions between the posterior and prior simulations derived from the assimilation of OMPS and TROPOMI formaldehyde observations over four key regions of China: the North China Plain, Yangtze River Delta, Pearl River Delta, and Sichuan Basin in 2019. Positive values indicate an increase in posterior emissions relative to the prior, while negative values indicate a decrease.

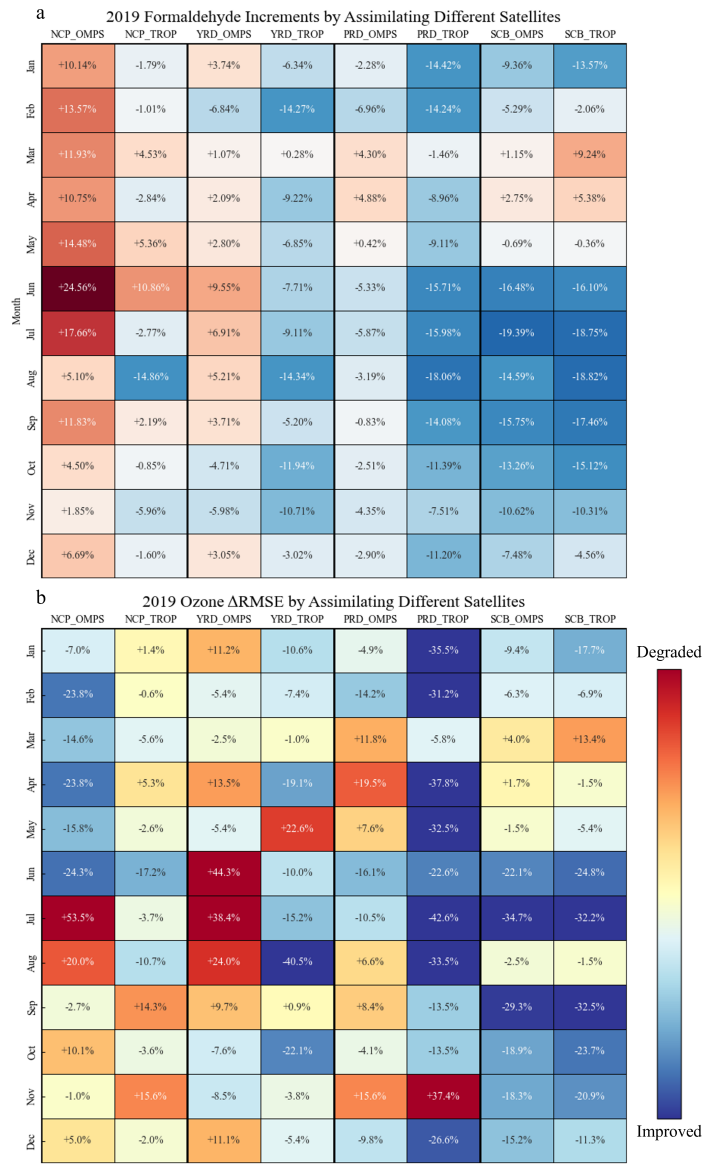


Figure 9. Monthly increments in (a) formaldehyde column concentrations between posterior and prior simulations and (b) the relative changes in MDA8 ozone RMSE (ΔRMSE) after assimilating OMPS and TROPOMI observations in 2019. Results are shown for the North China Plain, Yangtze River Delta, Pearl River Delta, and Sichuan Basin. Positive values indicate an increase relative to the prior, while negative values indicate a decrease.

in the Supplementary Information to provide additional context and support.

...

**NMVOC emissions**

...

In 2020, anthropogenic emissions in China were influenced by the COVID-19 pandemic, leading to observable changes. To better evaluate the general applicability of the proposed method, it is also necessary to conduct a comparative analysis for the pre-pandemic year of 2019. Figure ~~6 (a ). In spring, autumn and winter, anthropogenic emissions are generally higher than biogenic emissions while in summer biogenic sources are dominant. In January , April, and October,~~ S5 in the Supplement presents the total NMVOC emission increments for the four major regions in 2019, based on data assimilation of OMPS and TROPOMI observations. In the NCP region, strong consistency is again observed in June, with posterior emissions increasing by 57.71% and 30.09% from OMPS and TROPOMI assimilation, respectively, further confirming the underestimation of prior emissions in this period. In the ~~posterior estimates indicate that changesin total NMVOC emissions, constrained primarily by anthropogenic sources, are most prominent. Notably, in April and October, the southeastern coastal areas and Yunnan Province exhibit significantly elevated emission levels due to higher vegetation cover, with emissions in these regions approximately 10 to 20 $\times 10^{-4} kg/m^2$ higher in January. In contrast to the other three seasons, summer features high temperatures, intense radiation, and vigorous vegetation growth, which greatly increases biogenic emissions of isoprene and terpenes. Therefore, as shown in Figure 6 (c.3, d.3), biogenic NMVOC emissions in China peak in July(Wu et al., 2020) , with a significant expansion in the area covered by high values compared to other months. The total NMVOC emissions in eastern China in~~ YRD, February, October, and November are identified as consistent months, aligning with the consistent periods in 2020, suggesting a likely overestimation in the prior inventory during these months. In the PRD region, consistency is found in January, February, June, July~~increase from approximately 5 $\times 10^{-4}$ - 20 $\times 10^{-4} kg/m^2$ in the prior estimates to about 20 $\times 10^{-4}$ - 80 $\times 10^{-4} kg/m^2$ in the posterior estimates~~, November, and December, while in the SCB region, it occurs in January and from April to December. These consistent months largely overlap with those in 2020, though some differences are evident. For example, June and July emerge as new consistent months in PRD, while October and November remain consistent but exhibit notably smaller emission decreases compared to 2020. In SCB, April and May appear as additional consistent months, while the remaining consistent periods continue to exhibit decreases in emissions. Notably, from June to November, the two posterior datasets show an average decrease of 42.26% compared to the prior emissions, indicating a high probability of overestimation in the prior inventory for this region during that period.

...

**3.4 Impact of Formaldehyde Assimilation on $O_3$ Surface Concentration**

...

To more robustly substantiate this conclusion, it is necessary to examine whether similar features can also be identified in 2019. In that year, OMPS and TROPOMI satellite observations were assimilated independently to constrain NMVOC emissions. The posterior-prior increments from the OMPS- and TROPOMI-driven assimilations, together with the changes in MDA8 ozone $\Delta$RMSE, are presented in

Figure 8 of the Supplement. In NCP, March, May, and June are identified as consistent months, during which the ozone RMSE values decrease, with the most pronounced improvement occurring in June. In YRD, the consistent months are February, October, and November, where the ozone improvements are relatively limited but nevertheless show better agreement with ground-based observations. In PRD, the consistent months include January, February, and June-December; with the exception of August, September, and November, the ozone RMSE decreases in the other months, with notable improvements in June and July. In SCB, the two posterior datasets exhibit the highest level of consistency in 2019, with synchronous increases and decreases throughout the year. Ozone simulations in this region show better performance in all months except March and April, with particularly large improvements in June, July, and September-November, when the RMSE decreases by an average of 25.74%.

Across the four regions, 27 months are classified as consistent in 2019. Of these, 22 months exhibit improved ozone simulations, which corresponds to 81.48% of all consistent months, with both assimilations producing MDA8 ozone values closer to ground-based observations. This proportion differs from that of 2020 by only 0.23%, providing further evidence that ozone improvements are particularly significant in the months defined as consistent across the four regions.

...

**4 Summary and conclusion**

...

To further test the robustness of our approach, OMPS and TROPOMI satellite observations were independently assimilated to constrain NMVOC emissions for 2019 (Figure 7). The spatial distribution of formaldehyde hotspots is similar to 2020 but with overall higher concentrations. At the regional scale, most consistent months between OMPS- and TROPOMI-constrained results indicate that the prior inventory underestimates emissions in NCP and overestimates them in YRD, PRD, and SCB. Importantly, 22 of the 27 consistent months (81.48%) show reduced ozone RMSE, with the largest improvements in SCB, confirming that consistent cases are strongly associated with enhanced ozone simulation performance. These findings also lend greater confidence to the optimized NMVOC emissions during the consistent months in these regions.

**RC:** ***7) (Minor) Clarify whether the assimilation used OMPS only or both OMPS and TROPOMI. Identify which dataset(s) are considered "independent" validation.***

AR: Thank you for pointing this out. We have clarified the description of the assimilation datasets in the revised manuscript. Specifically, the monthly NMVOC emissions over China in 2020 are optimized by independently assimilating formaldehyde retrievals either from OMPS or from TROPOMI using our assimilation system. This means that two separate assimilation experiments are performed (OMPS-only and TROPOMI-only), rather than a combined assimilation. In Section 3.3, we use the TROPOMI measurements as independent data to validate the OMPS-based posterior, while in Section 3.4, we use ground-based surface ozone concentration measurements as independent data to validate both the TROPOMI- and OMPS-based posteriors. Additional remarks have been added in the revised manuscript to explicitly explain these validation strategies and avoid possible misunderstandings.

**Text in manuscript**

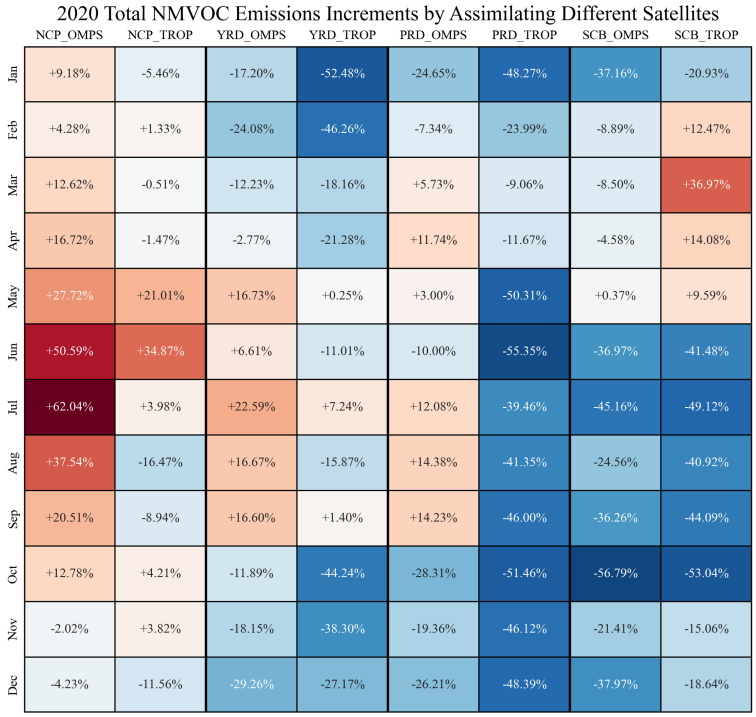


Figure 10. Monthly increments in total NMVOC emissions between the posterior and prior simulations derived from the assimilation of OMPS and TROPOMI formaldehyde observations over four key regions of China: the North China Plain, Yangtze River Delta, Pearl River Delta, and Sichuan Basin in 2020. Positive values indicate an increase in posterior emissions relative to the prior, while negative values indicate a decrease.

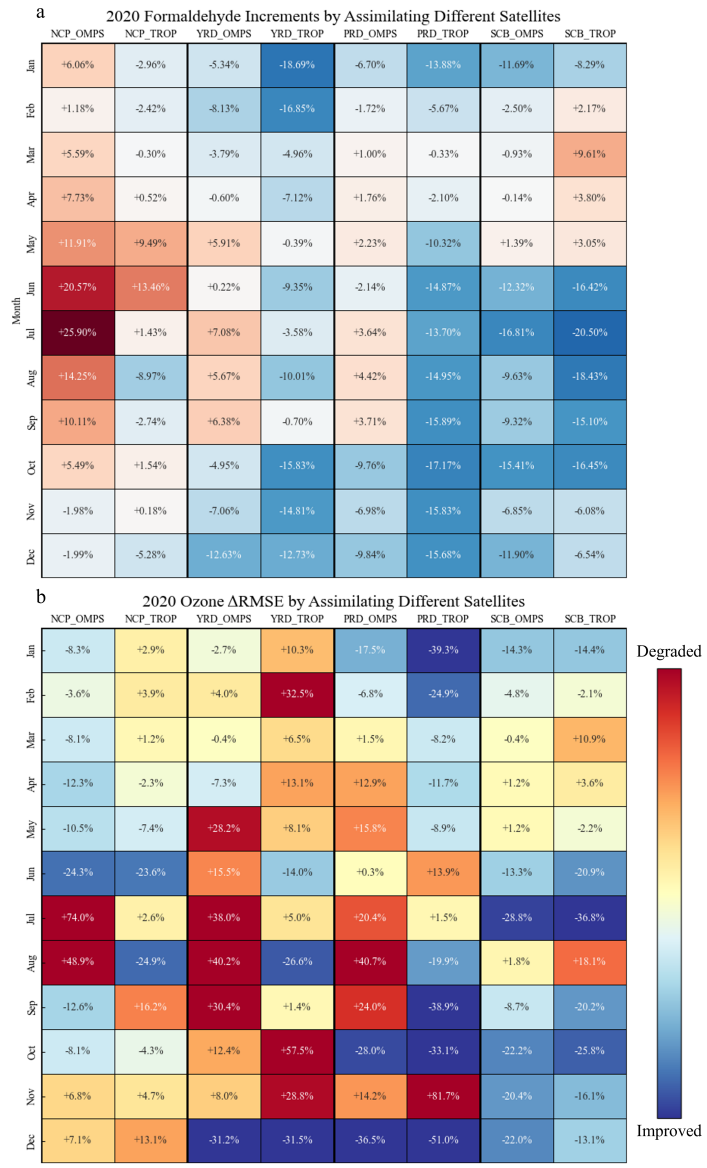


Figure 11. Monthly increments in (a) formaldehyde columns between posterior and prior simulations and (b) the relative changes in MDA8 ozone RMSE (ΔRMSE) after assimilating OMPS and TROPOMI observations in 2020. Results are shown for the North China Plain, Yangtze River Delta, Pearl River Delta, and Sichuan Basin. Positive values indicate an increase relative to the prior, while negative values indicate a decrease.

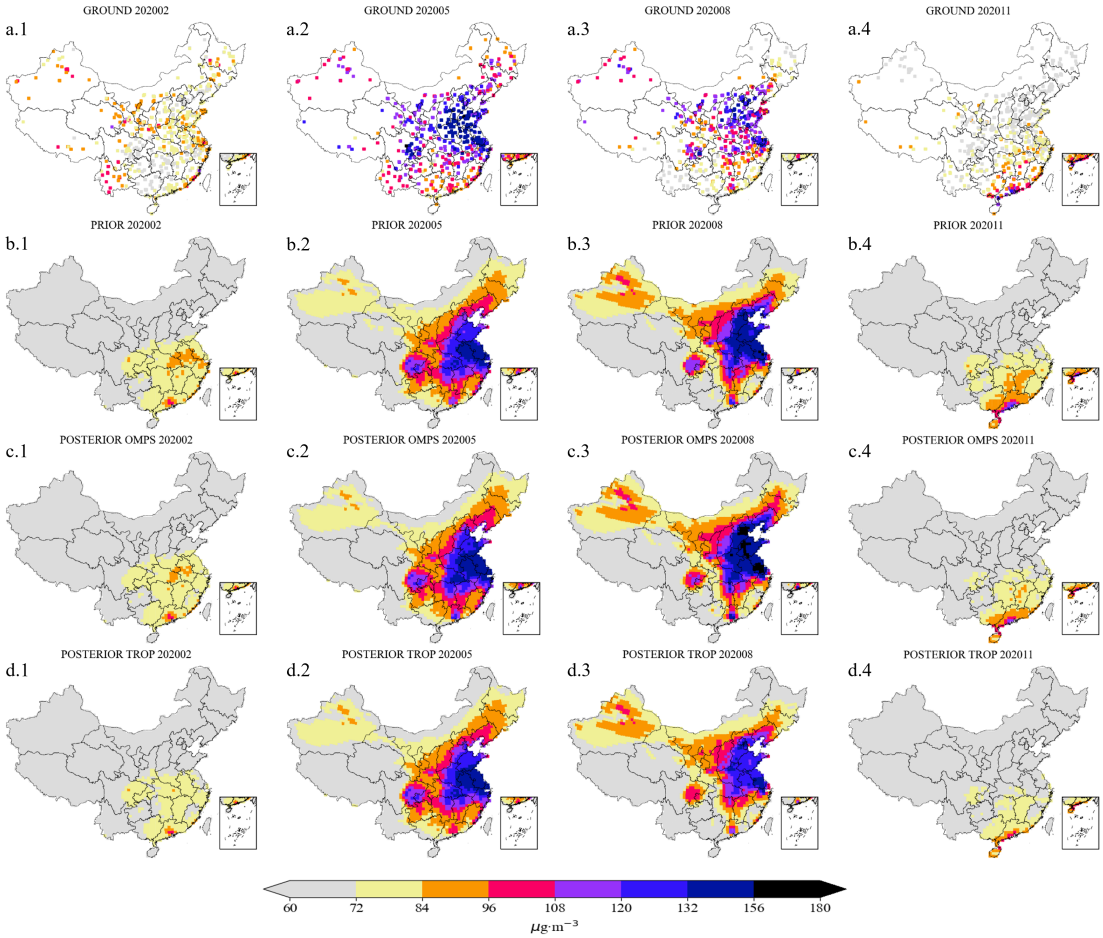


Figure 12. Spatial distributions of surface ozone concentrations in February, May, August, and November 2020. Panels (a.1-a.4) show ground-based observations, panels (b.1-b.4) show prior simulations, panels (c.1-c.4) show posterior simulations constrained by assimilating OMPS formaldehyde observations, and panels (d.1-d.4) show posterior simulations constrained by assimilating TROPOMI formaldehyde observations.

### 3.3 Formaldehyde columns evaluation

...

The prior and OMPS-driven posterior simulations of formaldehyde tropospheric columns were compared with the TROPOMI formaldehyde tropospheric columns to evaluate the changes in ~~Inner Mongolia, Tibet, and the northwest were minimal. This is because the assigned background uncertainty, which is proportional to~~ formaldehyde. Scatter plots together with statistical metrics ($R^2$, R, MAE, and RMSE) for the ~~prior emission intensity in these regions, was particularly low, leaving limited flexibility for adjustments in the assimilation. This can be best seen in Figure 2, these areas are depicted in gray on the map, with annual total emissions below 5 $\times 10^{-4} kg/m^2$, and the actual values for some grid points in these regions are even less than~~ whole country and four subregions in 2020 are presented in Figure 6. The prior simulation already shows reasonably good performance (a.1-e.1), with most points distributed close to the 1 $\times 10^{-4} kg/m^2$. ~~Though assimilating OMPS observations~~:1 line and exhibiting strong correlations with observations. Nevertheless, further improvements are still possible. After assimilating OMPS data, the posterior ~~simulation in these regionsstill remains low, resulting in little change. As illustrated in Figure 7 (a.2, a.3)~~results compared with TROPOMI show higher $R^2$ values across all regions, ~~the minimal changes in these areas also affected the national observation-minus-simulation discrepancies (root mean square error , RMSE), which decreased from 0.49 $\times 10^{16}$ molec/cm$^2$~~ indicating strengthened correlations. For China and NCP, the improvements are comparable, with $R^2$ increasing by about 0.027 (from 0.870 to ~~0.46 $\times 10^{16}$ molec/cm$^2$. However, as shown in Figure 7 (b.2) -(b.3) , when focused on the NCP region, the RMSE decreased from 0.53 $\times 10^{16}$ molec/cm$^2$~~ 0.897 for China, and from 0.774 to ~~0.37 $\times 10^{16}$ molec/cm$^2$effectively. As indicated in the time series plot in Figure 7 (a.1), due to the minimal changes in formaldehyde columns in Inner Mongolia, Tibet,~~ 0.812 for NCP). In the YRD, the improvement is more pronounced, with $R^2$ rising from 0.882 to 0.918, and the scatter around the regression line substantially reduced, with many outliers corrected. The most significant improvements occur in PRD and SCB, where $R^2$ increases by approximately 0.05. In these regions, the overestimations present in the prior simulations are effectively mitigated, particularly for high-value cases. In terms of RMSE and MAE, decreases are observed in all regions except NCP. A comparison between Figures (b.1) and (b.2) indicates improvements in the low- and ~~the northwest, the nationwide monthly average formaldehyde concentrations in the posterior results are still not high enough compared to TROPOMI data. However, when we plot the time series for the NCP region alone, the results are better. The~~ mid-value ranges, whereas substantial overestimations appear in the high-value range. This issue is likely related to the instrumental errors of OMPS observations, as discussed in Sections 2.3.1 and 3.2, which introduce considerable uncertainties.

...

### 3.4 Impact of formaldehyde assimilation on ozone surface concentration

~~The spatial distribution prior and posterior MDA8 surface $O_3$ concentration simulation, as well as the corresponding observations, are plotted in Figure 8. When comparing the prior MDA8 $O_3$ surface concentration results with data from 1602 stations nationwide, the prior results generally capture the main hot spots of~~ The spatial distributions of observed MDA8 ~~$O_3$ surface concentrations, especially in July, where they closely match the ground observations. However, in the other three months shown here, the performance is not as accurate as in July.~~

~~Figure 9 illustrates the evaluation of $O_3$ simulation in terms of different metrics, including probability~~

density (a), scatter plots (b), and correlation coefficients (c)ozone at ground stations (a.1-a.4), together with the prior (b.1-b.4) and posterior simulations based on OMPS and TROPOMI assimilation (c.1-c.4, d.1-d.4), are shown in Figure 12. As shown in Figure 9 (a), the frequency distribution histogram clearly demonstrates panels (b.1-b.4), pronounced ozone hotspots are observed in NCP (February, May, and August), YRD (May and August), PRD (May, August, and November), and SCB (May and August). This is very similar to the observations shown in panels (a.1-a.4). It indicates that the prior ground-level $O_3$ simulations systematically underestimate the observed values, whereas the posterior results effectively reduce this bias. This indicates that both the overall and regional simulations of surface $O_3$ concentrations have been significantly improved, especially in simulation captures the general patterns of ozone hotspots reasonably well, but notable biases remain. For example, ozone is clearly overestimated in PRD during February, May, and August, while underestimated in SCB during May and August. After assimilation with OMPS or TROPOMI, the NCP region. As can be seen in Figure 9 posterior MDA8 ozone simulations retain the overall hotspot distribution, but the direction and magnitude of changes vary by region. For instance, in August, ozone concentrations increase in NCP and PRD with OMPS assimilation but decrease with TROPOMI assimilation. In February, both assimilation results decrease in YRD, although the decrease is more pronounced in the TROPOMI-based results. Moreover, many regional changes are difficult to discern visually from the spatial maps alone, highlighting the necessity of using statistical metrics to quantitatively assess ozone variations.

The RMSE values between the simulated MDA8 ozone and the ground-based observations are calculated. To better visualize the assimilation benefits, the RMSE variation either assimilating the TROPOMI or assimilating the OMPS in the four key regions are also shown in Figure 11 (b). Larger decreases in RMSE (darker blue) indicate more significant improvements, with the posterior ozone being closer to ground-based observations; conversely, larger increases in RMSE (darker red) indicate degraded performance, with the posterior ozone diverging further from the observations. In those inconsistent cases where the OMPS and TROPOMI posterior increments exhibit opposite signs (i.e., one increases while the other decreases), ozone simulation improvement is not guaranteed. For instance, in NCP during January-April and July, in YRD during June and September, and in PRD during April, May, August, and September, one assimilation leads to improvement while the other indicates deterioration. Moreover, in several additional months both posteriors even show degradation, making it difficult to effectively evaluate the improvement in posterior ozone simulations. By contrast, ozone simulation improvements are clearly observed in consistent cases where the OMPS- and TROPOMI-constrained posteriors exhibit the same sign (i.e., both reductions in $\Delta$RMSE). In NCP, the RMSE (root mean square error) between the observed and simulated values decreasesfrom 24.44 $\mu$g/m$^3$ to 22.79 $\mu$g/m$^3$ for China and from 28.0 $\mu$gsubstantial improvements are observed in May and June, with the largest RMSE decrease in June, in agreement with the high-consistency pattern shown in Figure 11 (a). In YRD and PRD, RMSE decreases by more than 30% in December, representing the most significant improvement; in addition, PRD also shows clear improvements in January and October. These improvement months all correspond to periods of high consistency. In SCB, RMSE also decreases markedly during high-consistency months, including January, June, July, and September-December.

To further quantify ozone simulation improvements in consistent regions, statistics were performed for the months classified as consistent. Considering the similarity in monthly behavior between YRD and PRD, the two regions were combined in the analysis. The results indicate that the consistent regions include NCP in May-June, YRD/m$^3$ to 20.22 $\mu$gPRD in January-March and October-December, and SCB in January and June-December. Within these regions, except for March and November in

YRD/~~$m^3$ for the NCP region. As shown in Figure 9 (c), the correlation coefficients calculated based on the monthly average time series in the NCP region show a slight improvement, while the increase is more noticeable in the southern and northeastern regions. Spatial distributions of the MDA8 surface $O_3$ concentrations from GEOS-Chem model-simulated prior (a) and posterior (b) results, and from ground $O_3$ monitoring sites (c) in January (a.1)-(c.1), April (a.2)-(c.2), July (a.3)-(c.3), October 2020 (a.4)-(c.4). Frequency histogram of the difference between the ground monitoring observed and simulated $O_3$ surface concentrations over China and North China Plain in 2020 (a.1, a.2) and scatter plot of the observed vs. simulated $O_3$ surface concentrations using either prior data (b.1, b.3) or posterior data (b.2, b.4). The correlation coefficients calculated based on prior monthly averaged time series in 2020 (c.1), and the difference between posterior and prior correlation coefficients (c.2).~~ PRD and August in SCB, all other months show ozone simulation improvements. Overall, 13 out of the 16 consistent months exhibit improvements, accounting for 81.25%, with an average RMSE reduction of 24.7%. This result suggests that constraining NMVOC emissions through formaldehyde assimilation not only substantially improves formaldehyde simulations, but also exerts a positive impact on ozone simulations, with particularly significant improvements in regions and months characterized by high consistency.

**RC:** ***8) (Minor) Define acronyms such as "NCP" (North China Plain) and explicitly mention the study year (2020).***

AR: We thank the reviewer for this comment. In the revised Abstract, we have explicitly stated the study year (2020) and defined the four focus regions at first mention: the North China Plain (NCP), the Yangtze River Delta (YRD), the Pearl River Delta (PRD), and the Sichuan Basin (SCB). These acronyms are then used consistently throughout the manuscript.

**Text in manuscript**

**Abstract**

...

4DEnVar assimilation emission inversion system. The OMPS- and TROPOMI-driven assimilation yields consistent seasonal and regional increments in NMVOC emissions in general, but distinctions are also notable. A consistency analysis is introduced to assess the reliability of these two posterior emissions. Highly consistent increments are obtained in the North China Plain (May-June), the Yangtze River Delta and Pearl River Delta (January-March, ~~with the RMSE dropping from 0.52 to 0.37 $\times 10^{16}$ molec~~October-December), and the Sichuan Basin (January, June-December). These adjustments significantly improve surface ozone simulations, with 81.25% of consistent cases demonstrating reduced biases and an average RMSE reduction of 24.7%. These findings highlight the effectiveness of OMPS and TROPOMI formaldehyde assimilation, coupled with consistency analysis, in refining NMVOC emission estimates and enhancing ozone simulation accuracy. Similar promising results are achieved in the OMPS/~~$cm^2$. Validation using surface ozone observations also yielded favorable results, especially in NCP.~~TROPOMI-based NMVOC emission inversion in 2019.

**RC:** ***9) (Minor) The statement "validated through comparisons against the independent satellite measurements and the surface ozone measurements" should specify which satellite and ozone datasets were used and what "validated" means quantitatively.***

AR: We thank the reviewer for raising this point. In the revised Abstract, we removed the ambiguous phrase

"validated through comparisons against the independent satellite measurements and the surface ozone measurements" and replaced it with a clearer and quantitative description. Specifically, the validation is now based on posterior ozone simulations obtained from the OMPS-only and TROPOMI-only assimilation experiments, compared against surface ozone observations. Both assimilation cases yield reduced RMSE relative to the prior, with 81.25% of consistent cases showing bias reduction and an average RMSE decrease of 24.7%. This provides a more explicit and robust demonstration of validation through ozone metrics.

**Text in manuscript**

**Abstract**

...

4DEnVar assimilation emission inversion system. The OMPS- and TROPOMI-driven assimilation yields consistent seasonal and regional increments in NMVOC emissions in general, but distinctions are also notable. A consistency analysis is introduced to assess the reliability of these two posterior emissions. Highly consistent increments are obtained in the North China Plain (May-June), the Yangtze River Delta and Pearl River Delta (January-March, ~~with the RMSE dropping from 0.52 to 0.37 $\times 10^{16}$ molec~~October-December), and the Sichuan Basin (January, June-December). These adjustments significantly improve surface ozone simulations, with 81.25% of consistent cases demonstrating reduced biases and an average RMSE reduction of 24.7%. These findings highlight the effectiveness of OMPS and TROPOMI formaldehyde assimilation, coupled with consistency analysis, in refining NMVOC emission estimates and enhancing ozone simulation accuracy. Similar promising results are achieved in the OMPS/~~cm$^2$. Validation using surface ozone observations also yielded favorable results, especially in NCP.~~TROPOMI-based NMVOC emission inversion in 2019.

...

**3.3 Formaldehyde total columns evaluation**

...

The prior and OMPS-driven posterior simulations of formaldehyde tropospheric columns were compared with the TROPOMI formaldehyde tropospheric columns to evaluate the changes in ~~Inner Mongolia, Tibet, and the northwest were minimal. This is because the assigned background uncertainty, which is proportional to~~ formaldehyde. Scatter plots together with statistical metrics ($R^2$, R, MAE, and RMSE) for the ~~prior emission intensity in these regions, was particularly low, leaving limited flexibility for adjustments in the assimilation. This can be best seen in Figure 2, these areas are depicted in gray on the map, with annual total emissions below 5 $\times 10^{-4} kg/m^2$, and the actual values for some grid points in these regions are even less than~~ whole country and four subregions in 2020 are presented in Figure 6. The prior simulation already shows reasonably good performance (a.1-e.1), with most points distributed close to the 1$\times 10^{-4} kg/m^2$. ~~Though assimilating OMPS observations:~~1 line and exhibiting strong correlations with observations. Nevertheless, further improvements are still possible. After assimilating OMPS data, the posterior ~~simulation in these regionsstill remains low, resulting in little change. As illustrated in Figure 7 (a.2, a.3)~~results compared with TROPOMI show higher $R^2$ values across all regions, ~~the minimal changes in these areas also affected the national observation-minus-simulation discrepancies (root mean square error , RMSE), which decreased from 0.49 $\times 10^{16}$ molec/cm$^2$~~ indicating strengthened correlations. For China and NCP, the improvements are comparable, with $R^2$ increasing by about 0.027 (from 0.870 to ~~0.46 $\times 10^{16}$ molec/cm$^2$. However, as shown in Figure 7 (b.2) -(b.3) , when focused on the NCP region, the RMSE decreased from 0.53~~

~~$\times 10^{16}$ molec/cm$^2$~~ 0.897 for China, and from 0.774 to ~~0.37 $\times 10^{16}$ molec/cm$^2$ effectively.~~

~~As indicated in the time series plot in Figure 7 (a.1), due to the minimal changes in formaldehyde columns in Inner Mongolia, Tibet,~~ 0.812 for NCP). In the YRD, the improvement is more pronounced, with $R^2$ rising from 0.882 to 0.918, and the scatter around the regression line substantially reduced, with many outliers corrected. The most significant improvements occur in PRD and SCB, where $R^2$ increases by approximately 0.05. In these regions, the overestimations present in the prior simulations are effectively mitigated, particularly for high-value cases. In terms of RMSE and MAE, decreases are observed in all regions except NCP. A comparison between Figures (b.1) and (b.2) indicates improvements in the low- and ~~the northwest, the nationwide monthly average formaldehyde concentrations in the posterior results are still not high enough compared to TROPOMI data. However, when we plot the time series for the NCP region alone, the results are better. The~~ mid-value ranges, whereas substantial overestimations appear in the high-value range. This issue is likely related to the instrumental errors of OMPS observations, as discussed in Sections 2.3.1 and 3.2, which introduce considerable uncertainties.

...

**3.4 Impact of formaldehyde assimilation on ozone surface concentration**

...

Overall, 13 out of the 16 consistent months exhibit improvements, accounting for 81.25%, with an average RMSE reduction of 24.7%. This result suggests that constraining NMVOC emissions through formaldehyde assimilation not only substantially improves formaldehyde simulations, but also exerts a positive impact on ozone simulations, with particularly significant improvements in regions and months characterized by high consistency.

...

To more robustly substantiate this conclusion, it is necessary to examine whether similar features can also be identified in 2019. In that year, OMPS and TROPOMI satellite observations were assimilated independently to constrain NMVOC emissions. ... Ozone simulations in this region show better performance in all months except March and April, with particularly large improvements in June, July, and September-November, when the RMSE decreases by an average of 25.74%.

Across the four regions, 27 months are classified as consistent in 2019. Of these, 22 months exhibit improved ozone simulations, which corresponds to 81.48% of all consistent months, with both assimilations producing MDA8 ozone values closer to ground-based observations. This proportion differs from that of 2020 by only 0.23%, providing further evidence that ozone improvements are particularly significant in the months defined as consistent across the four regions.

**RC:** ***10) (Major) Provide more detail on bottom-up NMVOC emission uncertainties by sector (anthropogenic, biogenic, biomass burning).***

AR: We thank the reviewer for this important comment. In the revised manuscript, we have added detailed descriptions of sector-specific bottom-up NMVOC emission uncertainties. Following Souri et al. (2020), we assigned prior uncertainties of 150% for anthropogenic VOCs, 200% for biogenic VOCs, and 300% for biomass burning VOCs. These values reflect the larger variability typically associated with natural and fire emissions compared to anthropogenic sources. To incorporate these sectoral uncertainties into our inversion framework, they were combined using a weighted quadratic formulation, which yielded an overall uncertainty

of about 120%. Accordingly, the standard deviation of the multiplicative factor was set to 0.4. This treatment is now explicitly described in the manuscript with supporting references.

**Text in manuscript**

**2.5 Assimilation algorithm**

...

The uncertainty in the NMVOCs simulation is assumed to be attributed to errors in the emission inventories, and can be compensated using a spatially varying tuning factor $\alpha$:

$$f(i) = f_b(i) \cdot \alpha(i) \tag{23}$$

in here $f_b(i)$ denotes the NMVOC emission rate in the given grid cell $i$. The $\alpha$ values are defined to be random variables with a mean of 1.0, a minimum of 0.1 and a standard deviation ~~$\sigma_\alpha = 0.2$~~of 0.4, corresponding to a uniform 120% uncertainty applied to the total NMVOC emissions rather than sector-specific settings as adopted in previous studies (Choi et al., 2022; Jung et al., 2022; Souri et al., 2020) . The rationale for this choice is provided in the Supplement. This empirical value was found to provide sufficient spaces for resolving the observation-minus-simulation errors. A background covariance $\mathbf{B}_\alpha$ is formulated as a product of the constant standard deviation and a spatial correlation matrix $\mathbf{C}$:

$$\mathbf{B}_\alpha(i,j) = \sigma_\alpha \cdot \mathbf{C}(i,j) \tag{24}$$

where $\mathbf{C}(i,j)$ represents a distance-based spatial correlation between two $\alpha$s in the grid cell $i$ and $j$, and is defined as:

$$\mathbf{C}(i,j) = e^{-(d_{i,j}/l)^2/2} \tag{25}$$

where $d_{i,j}$ represents the distance between two grid cells $i$ and $j$. $l$ here denotes the correlation length scale which controls the spatially variability freedom of the $\alpha$s. A small value of $l$ ~~means more errors in fine scale could be resolved using the assimilation, while however requires more~~ indicates that the tuning factors $\alpha$s are less spatially correlated, thereby enabling emission optimization at a finer spatial scale. However, this also necessitates a larger number of ensemble runs to adequately represent the model realization from emission to simulation. An empirical ~~parameterl~~ parameter $l$ = 300 km which is used in Jin et al. (2023) to nudge the ammonia emission that has a rapid spatially variability is also taken in this study. With the covariance matrix $\mathbf{B}_\alpha$, the NMVOC emission background covariance $\mathbf{B}$ is obtained via a Schur Product:

$$\mathbf{B} = \mathbf{B}_\alpha \circ \mathbf{C} \tag{26}$$

...

**Supplement**

**1 Emission Uncertainty**

Following previous studies (Souri et al., 2020), sector-specific prior uncertainties for anthropogenic, biogenic, and biomass burning emissions can be combined into a total uncertainty using a weighted approach.

$$\sigma^2_{\text{total}} = f^2_{\text{anthro}} \cdot \sigma^2_{\text{anthro}} + f^2_{\text{biogenic}} \cdot \sigma^2_{\text{biogenic}} + f^2_{\text{bioburn}} \cdot \sigma^2_{\text{bioburn}} \tag{27}$$

Applying this method to the uncertainty values reported in earlier work, we obtained a total prior uncertainty of 120.22%. Accordingly, we set the standard deviation of the multiplicative factor to 0.4 in this study. To assess the validity of this simplification, we compared the sector-weighted prior emissions (Figure 5 (a)) with the prior emissions uniformly scaled by 120% (Figure 5 (b)). The two results are generally consistent, supporting the reasonableness of adopting a uniform total uncertainty in this study. Sector-specific inversion will be considered in future work.

**RC:** ***11) (Major) Expand the literature review of top-down VOC inversions. Important studies using various methods (e.g., Martin et al., 2003; Wells et al., 2020, 2022; Choi et al., 2022; Cao et al., 2018; Müller et al., 2024) are missing.***

AR: We thank the reviewer for this helpful suggestion. In the revised manuscript, we have expanded the literature review of top-down VOC inversions by incorporating the recommended studies and additional references. This provides a more comprehensive background and highlights both the methodological advances and the need for high-resolution emission optimization over China.

**Text in manuscript**

**1 Introduction**

...

Studies focusing on top-down NMVOC emission optimization over China remain relatively limited in recent years. Shim et al. (2005) assimilated formaldehyde observations from the GOME using a global Bayesian inversion to constrain isoprene emissions. Although China was included within their East Asia region, the analysis lacked region-specific focus and did not provide detailed characterization of emission patterns over China~~. Furthermore,~~ , and the coarse spatial resolution (4° ~~x~~ × 5°) in that study further limited the ability to resolve subregional emission features. Stavrakou et al. (2016) conducted a regional inversion in Eastern China using multi-year satellite formaldehyde data from GOME and OMI to constrain VOC emissions during the post-harvest burning period~~. Their~~ , and they indicated that the crop burning fluxes of VOCs in June ~~exceed~~ exceeded by a factor of ~~2~~ two the combined emissions from other anthropogenic activities in the NCP region from 2005 to 2012. Cao et al. (2018) conducted a relatively systematic satellite-based emission inversion study over China~~. They used~~ , using a 4DVar method and ~~assimilated~~ assimilating OMI and GOME-2A formaldehyde products to estimate monthly NMVOC emissions ~~over China~~ in 2007, ~~with a coarse spatial resolution~~

~~of~~ though the spatial resolution (4° ~~x~~ × 5°~~. Considering the increasingly stringent air pollution control policies and significant interannual variability in NMVOC emissionsin recent years, e.g. ~~)~~ was still too coarse. Choi et al. (2022) applied a 4DVar system to assimilate TROPOMI formaldehyde over East Asia, demonstrating the capability of high-resolution satellite data to capture regional and seasonal variability in VOC emissions, ~~the biomass buring emission is now reduced to a relatively low level~~but the analysis was conducted only for May-June. Beyond China, a number of important studies have advanced top-down VOC inversion methodologies: Palmer et al. (2003) pioneered the use of GOME formaldehyde observations in a Bayesian framework to constrain global isoprene emissions, laying the foundation for subsequent satellite-based VOC studies; Wells et al. (2020, 2022) further advanced this field by retrieving isoprene emissions from CrIS measurements and providing high-resolution constraints on VOC oxidation chemistry at the global scale; and Oomen et al. (2024) derived weekly top-down VOC fluxes over Europe from TROPOMI formaldehyde data using the MAGRITTEv1.1 model, providing improved constraints on isoprene, biomass burning, and anthropogenic VOC emissions. Considering the increasingly stringent air pollution control in China (Wu et al., 2024), there is an urgent need for high-resolution top-down ~~emission optimization over China~~NMVOC emission optimization.

**RC:** ***12) (Minor) p2, l2: Add a supporting reference for "became the major source region globally."***

AR: We thank the reviewer for pointing this out. We could not find a direct reference supporting the original phrasing "became the major source region globally." To avoid overstatement, we have revised the sentence to: "China has seen a rapid anthropogenic NMVOC emissions increase over the last three decades, gradually becoming one of the important contributors to global NMVOC emissions Li et al. (2019)." This modification provides a more accurate and properly referenced statement.

**Text in manuscript**

**1 Introduction**

...

Moreover, NMVOCs such as benzene, trichloroethylene, and chloroform are recognized for their toxicity (Billionnet et al., 2011; Lerner et al., 2012), and prolonged exposure to elevated concentrations can pose significant health risks (He et al., 2015). China has seen a rapid anthropogenic NMVOC emissions increase over the last three decades~~(Li et al., 2019), became the major source region globally~~, gradually becoming one of the important contributors to global NMVOC emissions (Li et al., 2019). Investigating NMVOC dynamics and their emission distributions is critical for addressing air pollution challenges in China (Yuan et al., 2013; Hao and Xie, 2018).

**RC:** ***13) (Minor) p2, l9: Include reference to biomass burning inventories.***

AR: Accepted. In the revised Introduction, we have added references to biomass burning emission inventories.

**Text in manuscript**

**1 Introduction**

...

NMVOCs are primarily released through anthropogenic activities, biogenic emissions, and biomass burning processes. Huge efforts have been devoted to constructing inventories recording these emissions

in a bottom-up way, such as the global Community Emission Data System (CEDS) (Hao and Xie, 2018), the regional Multi-resolution Emission Inventory for China (MEIC) (Li et al., 2019), and the Model of Emissions of Gases and Aerosols from Nature v2.1 (MEGAN) (Guenther et al., 2012). ~~These NMVOC emission inventories coupled~~ For biomass burning, widely used inventories include the Global Fire Emissions Database (GFED) and the Fire INventory from NCAR (FINN) (Wiedinmyer et al., 2011). Coupled with chemical transport models like GEOS-Chem (Ito et al., 2007) and WRF-Chem (Azmi et al., 2022), ~~are capable of reproducing the complex processes including~~ these inventories are widely used to simulate transport, deposition, and chemical ~~reactions. This not only helps to better quantify the environmental impact~~ transformations of NMVOCs, ~~but also provides essential tools for predicting future trends and making emission reduction~~ supporting air quality assessments and emission control strategies.

**RC:** ***14) (Minor) p2, l13: Mention both emission factors and activity data.***

AR: We thank the reviewer for the suggestion. In the revised Introduction, we have modified the text to mention both emission factors and activity data as key sources of uncertainty in bottom-up inventories.

**Text in manuscript**

**1 Introduction**

...

However, ~~the NMVOC emission factors required in the~~ bottom-up ~~method have large temporal and spatial variations, and this information is usually not widely available (Bo et al., 2008; Sharma et al., 2015). Additionally, due to the implementation of ever-stricter control measures targeting major industries, residential life~~estimates remain highly uncertain because both emission factors and activity data vary greatly in space and time and are often poorly constrained (Bo et al., 2008; Sharma et al., 2015). For anthropogenic sources, nationwide uncertainties of $\pm$68-78% have been reported due to variable activity data and emission factors under rapid structural transitions in industry, solvent use, and transportation ~~sectors~~ (Li et al., 2017, 2019). Biogenic emissions are even more uncertain, highly sensitive to land-cover, meteorology, and parameterizations, with Chinese BVOC estimates varying from 10 to 58.9 Tg C $yr^{-1}$ (Li et al., 2020; Wang et al., 2021; Pei et al., 2025).

**RC:** ***15) (Minor) Include references for VOC measurement techniques.***

AR: Thank you for the suggestion. References for VOC measurement techniques, including gas chromatography, mass spectrometry, Fourier transform infrared spectroscopy, and non-dispersive infrared analysis, have now been added in the revised manuscript.

**Text in manuscript**

**1 Introduction**

...

There are numerous well-established techniques for measuring the concentrations of various volatile organic compounds in the atmosphere. These include gas chromatography, mass spectrometry, Fourier transform infrared spectroscopy, and non-dispersive infrared analysis. While these methods are highly effective for meeting the requirements of experimental studies and real-time monitoring, their complex-

ity and the associated high labor costs pose significant challenges for long-term measurements or assessments across large spatial scales (Sakdapipanich and Insom, 2006; Cheng et al., 2017; Xing et al., 2022)

.

**RC:** ***16) (Minor) p2, l30-p3, l2: The discussion of glyoxal is unnecessary as it is not used in the study-suggest removing.***

AR: We thank the reviewer for this comment. While glyoxal is not directly used in this study, we have intentionally kept a brief discussion in the Introduction. This is to provide context that, among the numerous NMVOCs, only very few species can be retrieved from satellites on a long-term and large-scale basis. Formaldehyde and glyoxal are such species, but since formaldehyde products are more mature and of higher quality, we focus on formaldehyde in this study. We believe this comparison is important for justifying the choice of constraint species.

**RC:** ***17) (Minor) p4, l10: Remove the word "sources".***

AR: We thank the reviewer for carefully pointing out this wording error. We have revised the text accordingly in the manuscript.

**Text in manuscript**

**2 Data and methods**

~~This chapter~~

This section begins by introducing the GEOS-Chem model utilized for simulations in Section 2.1. Section 2.2 presents an overview of the ~~input emission sources for the model~~emissions used as the prior NMVOC inventories, including anthropogenic~~sources, biogenicsources~~, biogenic, and biomass burning inventories. Section 2.3 introduces the three satellite observations employed in the analysis in this study. In Section 2.4, the ground observations used for ~~$O_3$~~ ozone validation are presented. Section 2.5 ~~outlines a semi-variogram algorithm for a preliminary assessment of satellite observations quality, while Section 2.6 introduces the 4D-Var~~ introduces the 4DEnVar algorithm used for data assimilation.

**RC:** ***18) (Minor) p6, l4: Clarify what is meant by biogenic emissions being the main source-this may not apply to NCP.***

AR: We thank the reviewer for raising this point. To avoid potential misinterpretation, we have removed the statement about biogenic emissions being the main source in the revised manuscript.

**Text in manuscript**

**2 Data and methods**

...

For chemical species used in GEOS-Chem but not included in MEIC and anthropogenic NMVOC emissions outside China, we use the 2019 CEDS global inventory as a supplement. ~~The variations in NMVOC emissions mainly originate from biogenic sources.~~The prior estimates of biogenic NMVOC emissions in this study are obtained from the MEGAN 2.1 model (Guenther et al., 2012).

**RC:** ***19) (Minor) p6, l10: The claim about biogenic dominance is inconsistent with the previous sentence. Please reconcile.***

AR: We thank the reviewer for pointing this out. In the revised manuscript, we have corrected the wording to ensure consistency: both statements now indicate that anthropogenic sources dominate NMVOC emissions over China. The inconsistency in the earlier version has been removed.

**Text in manuscript**

**2 Data and methods**

...

Figure 13 (a) presents the prior NMVOC emission inventories for 2020, which primarily relies on the anthropogenic emission inventory from MEIC, supplemented by the CEDS inventory for species not included in MEIC. Additionally, ~~the biogenic emission inventory from~~ biogenic emissions are provided by MEGAN (offline calculation) ~~and the biomass burning inventory~~ for the year 2020 with an hourly temporal resolution, directly through the HEMCO emission component of GEOS-Chem; in this study, we did not run the MEGAN model separately. Biomass burning emissions are taken from GFED4~~are incorporated. The optimization of NMVOC emissions through the assimilation of formaldehyde observations will be conducted using these combined prior inventories.~~. The combination of these three sources is treated as the prior emission inventory used in the following NMVOC emission optimization.

**RC:** ***20) (Major) Section 2.3: Filtering criteria for OMPS and TROPOMI should be clearly described. Why are negative values removed only for TROPOMI? What thresholds are used for high outliers? What is the sensitivity to these choices?***

AR: We appreciate the referee for pointing out the improper filtering method used in the previous submission. In the original manuscript, our treatment of satellite data filtering was incorrect or improper, especially the practice of removing negative values directly, which could introduce a serious positive bias. In the revised version, we have substantially rewritten Section 2.3 to clearly describe and rigorously implement standardized quality control for OMPS, TROPOMI, and OMI data. For OMPS, we applied the recommended product screening, excluded outliers above $2 \times 10^{17}$ molecules $cm^{-2}$, applied thresholds for solar zenith angle, cloud fraction, air mass factors, and removed negative or unphysical values. For TROPOMI, we adopted the official QA value (>0.5) together with constraints on SZA, cloud radiance fraction, albedo, and snow/ice flags, and for OMI we followed established filtering practices considering row anomalies, cloud thresholds, and RMS fitting criteria. After filtering, all datasets were regridded to $0.5° \times 0.625°$ monthly means consistent with GEOS-Chem. To ensure robust sampling, we tested two schemes in which grid cells with fewer than 10 or fewer than 50 valid pixels were excluded; the differences are minor, particularly across the study regions, and are provided in the main text and Supplement. However, for OMI, the coverage becomes sparse after applying these thresholds, indicating that it does not support high-resolution assimilation studies.

**Text in manuscript**

**2.3.1 NOAA-20 OMPS**

...

In this study, the quality control scheme recommended in OMPS product documentation was applied~~when using OMPS data~~. Data points with formaldehyde column densities exceeding 2e17 molecules/$cm^2$ were excluded to minimize the impact of outliers. After removing outliers, we further excluded data points where the sum of formaldehyde column and twice the observation uncertainty

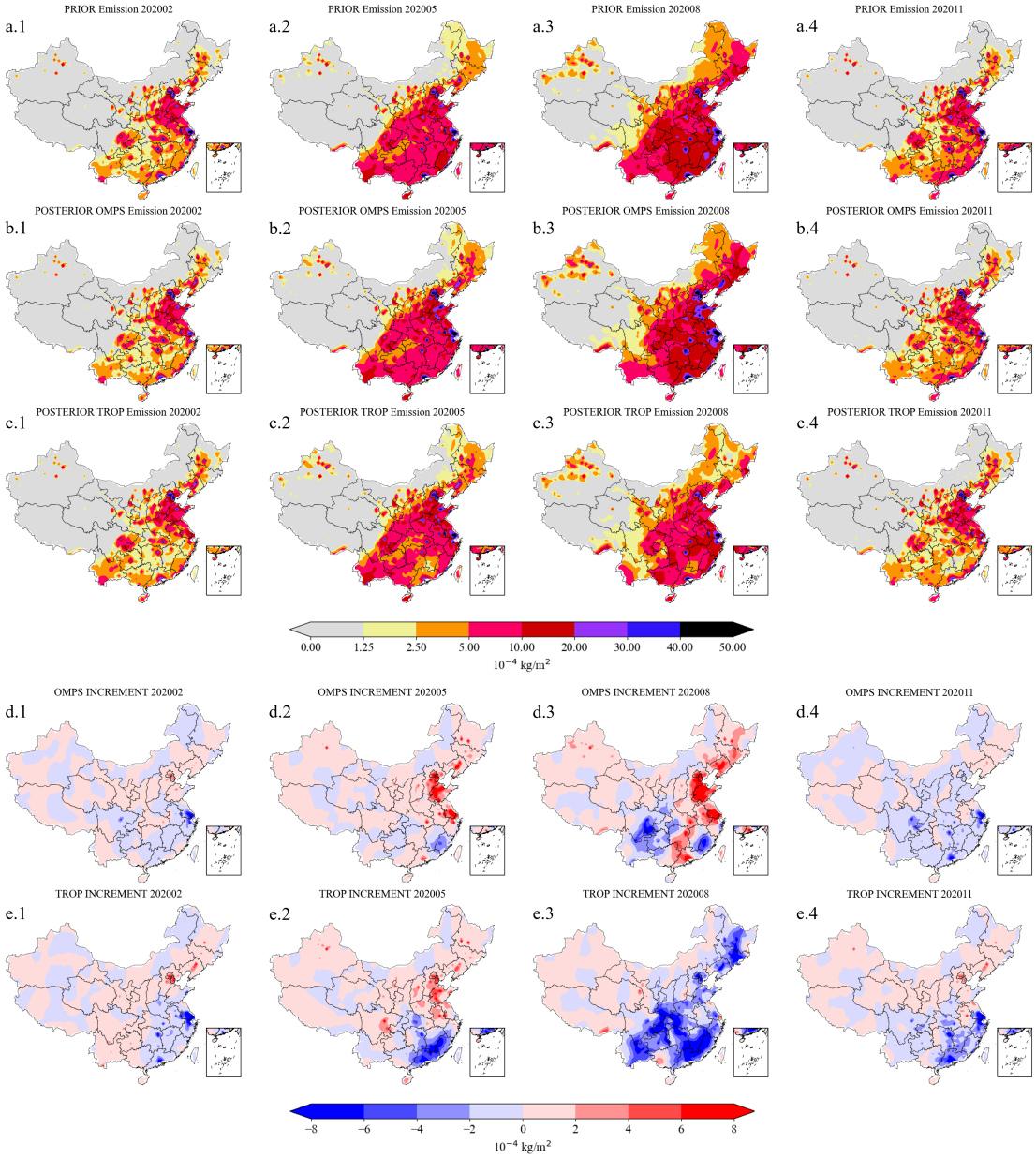


Figure 13. Spatial distributions of the total NMVOC emissions from the prior (a) and posterior (b) results in ~~January~~ February (a.1, b.1), ~~April~~ May (a.2, b.2), ~~July~~ August (a.3, b.3), ~~October~~ November (a.4, b.4) 2020. Panels (d.1-d.4) and (e.1-e.4) show the corresponding emission increments (posterior minus prior) derived from OMPS and TROPOMI assimilation.

was less than zero. Furthermore, the geometric air mass factors ($AMF_G$) were defined as follows:

$$AMF_G = sec(SZA) + sec(VZA) \tag{28}$$

Here, $SZA$ represents the solar zenith angle and $VZA$ denotes the viewing zenith angle. ~~After removing outliers, we further filtered out data points where the product of formaldehyde columns and three times the observation uncertainty was less than zero. Subsequently, data points were excluded if~~ Additional data screening was applied by excluding observations with $SZA$ ~~exceeded~~ greater than 70°, ~~the~~ an air mass factor ~~was~~ less than 0.1, ~~the~~ a geometric air mass factor ~~exceeded 5, or the cloud fraction surpassed~~ greater than 4, a cloud fraction exceeding 0.4~~. Snapshots of filtered~~ , or with positive snow and ice fractions. All screened data were then averaged to a spatial resolution of 0.5° latitude × 0.625° longitude on a monthly basis, consistent with the GEOS-Chem model configuration. To make a fair comparison between the observed and simulation formaldehyde column concentration in the assimilation, we further imposed constraints on the number of observations within each grid cell. Specifically, two filtering schemes were tested, in which grid cells with fewer than 10 or fewer than 50 original observations were excluded. The OMPS formaldehyde columns ~~is~~ after applying the threshold of 50 are shown in Figure ~~1(e~~1 (c), while the results with the threshold of 10 are provided in the Supplement. The differences between the two filtering schemes are minor, particularly across the four study regions considered in this work.

...

### 2.3.2 Sentinel-5P TROPOMI

...

When using Level 2 TROPOMI formaldehyde data for the validation in this ~~paper, we excluded only negative values and excessively large outliers to ensure data coverage. Examples of filtered TROPOMI formaldehyde columns are shown in Figure 1(d)~~study, we applied the recommended quality assurance filtering by retaining only pixels with a qa value greater than 0.5. This criterion ensures the exclusion of error flags and requires that the cloud radiance fraction at 340 nm is below 0.5, the solar zenith angle (SZA) does not exceed 70°, the surface albedo is below 0.2, no snow or ice warning is present, and the air mass factor (AMF) is larger than 0.1. The TROPOMI product provides vertical information on 34 layers, but the retrieval is primarily sensitive to the troposphere and thus reports the formaldehyde tropospheric column. After filtering, the TROPOMI observations were aggregated to monthly means on a 0.5° × 0.625° grid, ensuring consistency with the resolution used in the GEOS-Chem simulations. In addition, we further constrained the number of observations per grid cell: Figure 1 (d) shows the results after excluding grid cells with fewer than 50 observations, while the results with a threshold of 10 are also provided in the Supplement. The differences between the two filtering schemes are minor, particularly over the study regions.

...

### 2.3.3 Aura OMI

...

In this study, we use the OMI/Aura formaldehyde Total Column Daily L2 Global Version 3 prod-

uct (Chance, 2014)~~is also used for the observation sources in this paper. The retrieval algorithm for this product is based on a nonlinear least-squares fitting technique, which calculates the slant column density (SCD) . The SCD is then converted to vertical column density (VCD) using air mass factors ($AMF$). Since atmospheric formaldehyde is primarily concentrated in the troposphere, the total VCD can be regarded as the tropospheric VCD of formaldehyde (Duncan et al., 2010). In practical applications, data with a cloud fraction greater than or equal to~~ . In order to minimize the influence of poor-quality data, we applied strict quality filtering. Only pixels with cloud fraction $\leqslant$ 0.3~~are further excluded~~, solar zenith angle $\leqslant 70°$, and a main data quality flag = 0 were retained. To avoid poor-quality measurements at large pixel sizes, the five marginal pixels on each side of the swath were discarded, and only pixels within rows 6-55 were used (Zhu et al., 2017; Xue et al., 2020) . Because OMI has experienced a row anomaly since 2007, pixels with Xtrack quality flags = 0 were further selected to eliminate its impact. Additionally, given the large uncertainties in formaldehyde retrievals, pixels with a fitting root mean square (RMS) $\leqslant 0.003$ were retained to remove most outliers (Souri et al., 2017).

The OMI observations are then aggregated to monthly means on a $0.5° \times 0.625°$ grid, consistent with the GEOS-Chem model resolution. To ensure sufficient sampling per grid cell, we also applied two filtering schemes based on the number of observations, excluding grid cells with fewer than 10 or fewer than 50 valid pixels. Unlike OMPS and TROPOMI, however, OMI shows a strong reduction in data coverage under these constraints, and the product becomes sparse after applying the threshold of 50 observations. This indicates that OMI suffers from insufficient sampling density in China for high-resolution assimilation. The vertical profile correction of OMI formaldehyde was conducted using the same approach as applied to OMPS, by recalculating AMF with model-simulated vertical profiles.

**RC:** ***21) (Major) Section 2.6: Provide full details on the inversion algorithm, adjoint model (if used), regularization, convergence, and assimilation setup for multiple satellite datasets.***

AR: We thank the reviewer for this important comment. As explained in detail in our response to RC 4, we have clarified the inversion framework as a 4DEnVar system, which is adjoint-free and based on ensemble linearization of the GEOS-Chem formaldehyde simulation. Additional details concerning the algorithm, regularization, convergence, and assimilation setup have been added in the revised manuscript and the Supplement.

**Text in manuscript**

**2.5 Assimilation algorithm**

This study employs the four-dimensional ensemble variational (4DEnVar) methodology to ~~assimilate formaldehyde observations to constrain NMVOC emissions~~ optimize NMVOC emissions with satellite formaldehyde observations. The goal of ~~this~~ the assimilation is to find the most likely estimate of the state vector, which is the monthly NMVOC emission inventories $\boldsymbol{f}$ over the entire model domain. Note that $\boldsymbol{f}$ represents the vector of total NMVOC emissions, rather than separately gridded anthropogenic, biogenic, or biomass burning VOC emissions. To optimize emissions from these three sectors, additional observations or a well-defined spatial correlation structure are required, which are not available in this study. The prior estimate $\boldsymbol{f}_b$ is from the inventories described in Section 2.2, and the formaldehyde concentration observations $\boldsymbol{y}$ are described in Section 2.3. Mathematically,

assimilation is performed via minimizing the cost function $J$ as follows:

$$\mathcal{J}(\boldsymbol{f}) = \frac{1}{2}(\boldsymbol{f} - \boldsymbol{f}_b)^T \mathbf{B}^{-1}(\boldsymbol{f} - \boldsymbol{f}_b) + \frac{1}{2}\{\boldsymbol{y} - \mathcal{HM}(\boldsymbol{f})\}^T \mathbf{O}^{-1}\{\boldsymbol{y} - \mathcal{HM}(\boldsymbol{f})\} \quad (29)$$

The cost function $\mathcal{J}$ is the sum of two ~~part~~parts: background and observation penal term. The background term quantifies the difference between the optimal $\vec{f}$ and the prior emission inventories $\vec{f}_b$, while the observation term calculates the difference between the simulation driven by $\vec{f}$ and the satellite observations $\vec{y}$. In addition to the $\boldsymbol{f}_b$ that represents the prior NMVOC emission vector calculated from the anthropogenic, biogenic, and biomass burning sources as been illustrated in Section 2.2. The uncertainty in the NMVOCs simulation is assumed to be attributed to errors in the emission inventories, and can be compensated using a spatially varying tuning factor $\alpha$:

$$f(i) = f_b(i) \cdot \alpha(i) \quad (30)$$

in here $f_b(i)$ denotes the NMVOC emission rate in the given grid cell $i$. The $\alpha$ values are defined to be random variables with a mean of 1.0, a minimum of 0.1 and a standard deviation ~~$\sigma_\alpha = 0.2$~~of 0.4, corresponding to a uniform 120% uncertainty applied to the total NMVOC emissions rather than sector-specific settings as adopted in previous studies (Choi et al., 2022; Jung et al., 2022; Souri et al., 2020) . The rationale for this choice is provided in the Supplement. This empirical value was found to provide sufficient spaces for resolving the observation-minus-simulation errors. A background covariance $\mathbf{B}_\alpha$ is formulated as a product of the constant standard deviation and a spatial correlation matrix $\mathbf{C}$:

$$\mathbf{B}_\alpha(i,j) = \sigma_\alpha \cdot \mathbf{C}(i,j) \quad (31)$$

where $\mathbf{C}(i,j)$ represents a distance-based spatial correlation between two $\alpha$s in the grid cell $i$ and $j$, and is defined as:

$$\mathbf{C}(i,j) = e^{-(d_{i,j}/l)^2/2} \quad (32)$$

where $d_{i,j}$ represents the distance between two grid cells $i$ and $j$. $l$ here denotes the correlation length scale which controls the spatially variability freedom of the $\alpha$s. A small value of $l$ ~~means more errors in fine scale could be resolved using the assimilation, while however requires more~~ indicates that the tuning factors $\alpha$s are less spatially correlated, thereby enabling emission optimization at a finer spatial scale. However, this also necessitates a larger number of ensemble runs to adequately represent the model realization from emission to simulation. An empirical ~~parameterl~~ parameter $l$ = 300 km which is used in Jin et al. (2023) to nudge the ammonia emission that has a rapid spatially variability is also taken in this study. With the covariance matrix $\mathbf{B}_\alpha$, the NMVOC emission background covariance $\mathbf{B}$ is

obtained via a Schur Product:

$$\mathbf{B} = \mathbf{B}_{\alpha} \circ \mathbf{C} \tag{33}$$

In the observation term, $\boldsymbol{y}$ is the observation vector, representing satellite observations, $\mathcal{M}$ is the GEOS-Chem model driven by emissions $\boldsymbol{f}$, $\mathcal{H}$ is the observation operator that ~~transfer the three dimensional~~ transfers the three-dimensional concentration into the observational space, and $\mathbf{O}$ is the observation covariance matrix. In this study, the assimilated observations include the OMPS total columns and TROPOMI tropospheric columns. A distinct observation operator $\mathcal{H}$ is configured to enable a fair comparison of the observation-minus-simulation mismatch. The satellite formaldehyde observations are assumed to be independent, therefore $\mathbf{O}$ is a diagonal matrix. The diagonal value here is calculated as:

$$\sigma_{\text{total}} = \sqrt{\sigma^2_{\text{instrument}} + \sigma^2_{\text{represent}}} \tag{34}$$

In ~~the~~ Equation 34, $\sigma_{\text{total}}$ is defined as the total uncertainty, which is the square root of the sum of the squares of the instrument uncertainty $\sigma_{\text{instrument}}$ from the formaldehyde observations and the representative uncertainty $\sigma_{\text{represent}}$ introduced when processing the data into monthly averages. The representative uncertainty $\sigma_{\text{represent}}$ is represented by the standard deviation of the data.

~~With the assimilation-based emission inversion system above, we conducted three sets of experiments to explore the benefits to emission optimization. These experiments involved assimilating OMPS data and validating the assimilation results using TROPOMI, assimilating TROPOMI data, and finally assimilating the combined OMPS and TROPOMI data by averaging them. In the subsequent results, we primarily analyze the results of the first set of experiments, while the detailed inventories of the latter two experiments are archived in~~ The spatial distribution of the total uncertainty is provided in Figure **??** in the Supplement.

The assimilation methodology used in this paper is the four-dimensional ensemble variational (4DEnVar). Different from the classic 4DVar that requires adjoint in the cost function minimization, 4DEnVar emulates the GEOS-Chem formaldehyde simulating model using an ensemble-based linear approximation and hence is adjoint-free. The method is first proposed by Liu et al. (2008) and successfully implemented in our recent dust aerosol (Jin et al., 2021) and ammonia emission inversion (Jin et al., 2023; Xia et al., 2025) . The detailed procedures for minimizing the cost function Equation 29 are illustrated in section 'Minimization of the Cost Function in 4DEnVar' in supplementary material.

**Supplement**

## 2 Minimization of the Cost Function in 4DEnVar

The minimization of the cost function follows the 4DEnVar processes. An ensemble of emission inventory is generated randomly using the prior emission vector $f$ and the assumed emission error

covariance $\mathbf{B}$:

$$[f_1, \ldots, f_N] \tag{35}$$

An ensemble of GEOS-Chem model simulations is then forward run with the ensemble emission inventories in parallel:

$$[\mathcal{M}(f_1), \ldots, \mathcal{M}(f_N)] \tag{36}$$

Denote the emission ensemble perturbation matrix by:

$$F' = \frac{1}{\sqrt{N-1}}[f_1 - \bar{f}, \ldots, f_N - \bar{f}] \tag{37}$$

and the mean of ensemble simulation by:

$$\mathcal{M}(\bar{f}) = \frac{1}{N}\sum_{i=1}^{N}\mathcal{M}(f_i) \tag{38}$$

where $\bar{f}$ is the mean of the ensemble emission inventories. In the 4DEnVar assimilation algorithm, the optimal emission $f$ is defined as a weighted sum of the columns of the perturbation matrix $F'$ using weights from a control variable vector $w$:

$$f = \bar{f} + F'w \tag{39}$$

The cost function could then be reformulated as:

$$\mathcal{J}(w) = \frac{1}{2}w^T w + \frac{1}{2}\left\{H\mathcal{M}'w + H\mathcal{M}(\bar{f}) - y\right\}^T \mathbf{O}^{-1}\left\{H\mathcal{M}'w + H\mathcal{M}(\bar{f}) - y\right\} \tag{40}$$

where $\mathcal{M}$ is the linearization of the GEOS-Chem formaldehyde simulating model required for cost function minimization, and is approximated by:

$$\mathcal{M}'F' \approx \frac{1}{\sqrt{N}}\left[\mathcal{M}(f_1) - \mathcal{M}(\bar{f}), \ldots, \mathcal{M}(f_N) - \mathcal{M}(\bar{f})\right] \tag{41}$$

With the uncertainty in emission transferred into the observation space, the minimum of the cost function in Equation 40 could then be directly calculated, and the posterior emission $f$ subsequently updated.

$$m_z = \frac{M_z^m - B_z}{M^m - B} \tag{42}$$

Here $M_z^m$ represents the modeled concentration of formaldehyde at altitude $z$, $B_z$ is the background concentration of formaldehyde at the same altitude, $M^m$ represents the total modeled concentration of formaldehyde in the atmosphere, and $B$ is the total background concentration.

$$A_z^a = \frac{1}{N}\frac{\hat{X}^a - B}{\hat{X}^l - B} \tag{43}$$

Here $X_z^a$ represents the a priori (or assumed) concentration of formaldehyde at altitude $z$, $B_z$ is again the background concentration at the same altitude, $\hat{X}^a$ is the total a priori concentration, and $N$ is a normalization factor ensuring the matrix $A_z^a$ sums correctly to account for all altitudes.

**RC:** ***22) (Minor) p9, l2-5: Add references for each cited method.***

AR: We thank the reviewer for this comment. The section referring to semi-variogram analysis (p9, l2-5) has been removed in the revised manuscript following Reviewer #2's suggestion.

**RC:** ***23) (Minor) p9, l14: Add publication year for Souri et al.***

AR: The section referring to semi-variogram analysis, where the citation of Souri et al. appeared, has been removed in the revised manuscript following Reviewer #2's suggestion. Nevertheless, we have carefully checked the remaining references to ensure that all citations include publication years, so this issue will not occur elsewhere.

**RC:** ***24) (Minor) p9, l15: Replace "superiority" with a specific performance attribute (e.g., lower noise, finer resolution).***

AR: We thank the reviewer for this comment. The section on semi-variogram analysis, where the term "superiority" appeared, has been removed in the revised manuscript following Reviewer #2's suggestion.

**RC:** ***25) (Major) Begin the discussion by comparing OMPS and TROPOMI retrievals pre-assimilation. Quan-***

***tify differences and their potential impact.***

AR: We thank the reviewer for this important suggestion. As detailed in our response to RC 2, we have added a pre-assimilation comparison between OMPS and TROPOMI retrievals, quantified their differences, and discussed the potential impacts on the assimilation results in the revised manuscript.

**Text in manuscript**

~~3.1 Semi-variogram analysis~~**3.1 Satellite data evaluation**

...

Uncertainty is a key component in the assimilation process and serves as a crucial indicator of satellite data quality. Figure 3 illustrates the vertical distribution of retrieval uncertainties. In the mid- to upper troposphere (200-600 hPa), OMPS and OMI show comparable levels of uncertainty. However, below 600 hPa, OMPS uncertainties become substantially larger, likely due to cloud contamination and retrieval algorithm approximations (González Abad et al., 2016; Nowlan et al., 2023). As shown in ~~the four interpolated results in Figure 3, the spatial distribution of high formaldehyde values is consistently captured across different horizontal resolutions, either by the satellite observations in Figure 3~~Supplementary Figure **??**, the overall uncertainty of OMPS is significantly higher than that of the other two satellite datasets. At first glance, OMI data may appear superior, but this advantage largely results from strict filtering, which excludes a substantial fraction of problematic data. As illustrated in Supplementary Figure 4 (a, b~~, c)or by GEOS-Chem simulation in panel (d). These hot spots are particularly prominent in the North China Plain (NCP) and Jiangsu-Zhejiang-Shanghai regions. However, at the higher resolution of 0.5° x 0.5°, OMI formaldehyde data exhibits noticeable noise all over China and lacks the spatial continuity observed in TROPOMI, OMPS, and GEOS-Chem datasets. The significant spatial variability in the NMVOC emission field might account for the discontinuity observed in OMI formaldehyde data . However, this discontinuity contradicts the model simulation and the other two satellite products obtained from the more advanced instruments. Moreover, such discontinuities are not observedin OMI formaldehyde retrievals over the United States, where (Kaiser et al., 2018) demonstrated continuous and high-quality data. Therefore, the discrepancies observed in China may be attributed to uncertain input parameters, such as aerosols and surface albedo. OMI formaldehyde retrievals with larger spatial grid intervals (2° × 2° )~~, applying a threshold of 50 observations per grid cell drastically reduces spatial coverage, rendering OMI unsuitable for national-scale assimilation. Previous studies that assimilated OMI over China have typically interpolated the data to coarser resolutions to ensure applicability (Cao et al., 2018; Miyazaki et al., 2020). Therefore, only OMPS and ~~4° x 4°) exhibit increased continuity and smoothness, as shown in Figure 3(a). This improvement is attributed to spatial averaging, which effectively filters out white noise (Lee, 1980).~~

...

**3.3 Formaldehyde ~~total~~ columns evaluation**

The spatial distributions of formaldehyde columns in February, May, August, and November 2020 are shown in Figure ~~1 (a) and (b), GEOS-Chem simulated the prior and posterior estimates of formaldehyde for four months of the year 2020 over China. In Figure 1 (a) , the prior results exhibit a spatial distribution similar to satellite observations . When compared to OMPS and~~ 1. Panels (a.1-a.4) display the prior simulations of tropospheric columns, (b.1-b.4) present the posterior simulations of tropospheric columns assimilated by OMPS, (c.1-c.4) show the OMPS satellite observations of total columns, and (d.1-d.4) illustrate the TROPOMI satellite observations of tropospheric columns.

In addition, the prior ~~results accurately reproduce high-value features in most regions, including Yunnan-Guizhou, Guangxi-Guangdong, NCP, the southeastern coast, and the northeast. However, the previous simulation did not accurately represent the actual formaldehyde levels. Specifically, it underestimated formaldehyde concentrations to varying degrees across different regions. By assimilating OMPS formaldehyde columns, improvement was obtained steadily in the posterior simulations. Nationwide, the posterior formaldehyde columns were raised by approximately 50%. Comparing to TROPOMI data used as independent measurements, the~~ and posterior simulations of total columns for 2020 are also provided in the Supplementary Figure 2. As indicated by the vertical profiles in Figure 3, formaldehyde ~~levels~~ is mainly distributed below the tropopause. Comparisons between the prior and posterior results show that the differences between total and tropospheric columns are relatively small. Regarding the spatial patterns, high formaldehyde values in February are concentrated in the NCP~~region were raised from less than 1.2 $\times 10^{16}$ molec/cm$^2$ to around 2.4 $\times 10^{16}$ molec/cm$^2$ in January, closer to the observed values either from OMPS and TROPOMI. The~~ , YRD, and PRD regions, with the posterior results showing an expanded high-value ~~features in Yunnan-Guizhou became more prominent in April, and significant improvements were also observed in the southeastern coast, NCP, and the northeast in July and October. However,~~ area in the NCP but a reduced coverage in the YRD. In May, overall concentrations increase nationwide, with particularly pronounced growth in the NCP and PRD. In August, concentrations increase in the NCP, YRD, and PRD, while they decrease in the SCB. In November, the changes are modest, but all four regions exhibit reduced concentrations.

**RC:** ***26) (Major) Clarify whether the system constrains species and sectors independently. If so, discuss implications for chemical speciation and whether the results are physically plausible.***

AR: We thank the reviewer for this suggestion. Our study focuses on optimizing the total NMVOC emissions rather than sector-specific sources. This has now been clarified in the manuscript.

**Text in manuscript**

**2.5 Assimilation algorithm**

...

This study employs the four-dimensional ensemble variational (4DEnVar) methodology to ~~assimilate formaldehyde observations to constrain NMVOC emissions~~ optimize NMVOC emissions with satellite formaldehyde observations. The goal of ~~this~~ the assimilation is to find the most likely estimate of the state vector, which is the monthly NMVOC emission inventories $\boldsymbol{f}$ over the entire model domain. Note that $\boldsymbol{f}$ represents the vector of total NMVOC emissions, rather than separately gridded anthropogenic, biogenic, or biomass burning VOC emissions. To optimize emissions from these three sectors, additional observations or a well-defined spatial correlation structure are required, which are not available in this study.

**RC:** ***27) (Major) Discuss the impact of COVID-19 on emissions in 2020 and how it relates to your findings.***

AR: We thank the reviewer for this important comment. As explained in RC 6, we have addressed the impact of COVID-19 by comparing 2020 with 2019, and clarified how this relates to our findings in the revised manuscript.

**Text in manuscript**

**1 Introduction**

...

In this study, we focus on the year 2020 for the main analysis, while results for 2019 are also presented in the Supplementary Information to provide additional context and support.

...

**NMVOC emissions**

...

In 2020, anthropogenic emissions in China were influenced by the COVID-19 pandemic, leading to observable changes. To better evaluate the general applicability of the proposed method, it is also necessary to conduct a comparative analysis for the pre-pandemic year of 2019. Figure ~~6 (a ). In spring, autumn and winter, anthropogenic emissions are generally higher than biogenic emissions while in summer biogenic sources are dominant. In January , April, and October,~~ S5 in the Supplement presents the total NMVOC emission increments for the four major regions in 2019, based on data assimilation of OMPS and TROPOMI observations. In the NCP region, strong consistency is again observed in June, with posterior emissions increasing by 57.71% and 30.09% from OMPS and TROPOMI assimilation, respectively, further confirming the underestimation of prior emissions in this period. In the ~~posterior estimates indicate that changesin total NMVOC emissions, constrained primarily by anthropogenic sources, are most prominent. Notably, in April and October, the southeastern coastal areas and Yunnan Province exhibit significantly elevated emission levels due to higher vegetation cover, with emissions in these regions approximately 10 to 20 $\times 10^{-4} kg/m^2$ higher in January. In contrast to the other three seasons, summer features high temperatures, intense radiation, and vigorous vegetation growth, which greatly increases biogenic emissions of isoprene and terpenes. Therefore, as shown in Figure 6 (c.3, d.3), biogenic NMVOC emissions in China peak in July(Wu et al., 2020) , with a significant expansion in the area covered by high values compared to other months. The total NMVOC emissions in eastern China in~~ YRD, February, October, and November are identified as consistent months, aligning with the consistent periods in 2020, suggesting a likely overestimation in the prior inventory during these months. In the PRD region, consistency is found in January, February, June, July~~increase from approximately 5 $\times 10^{-4}$ - 20 $\times 10^{-4} kg/m^2$ in the prior estimates to about 20 $\times 10^{-4}$ - 80 $\times 10^{-4} kg/m^2$ in the posterior estimates~~, November, and December, while in the SCB region, it occurs in January and from April to December. These consistent months largely overlap with those in 2020, though some differences are evident. For example, June and July emerge as new consistent months in PRD, while October and November remain consistent but exhibit notably smaller emission decreases compared to 2020. In SCB, April and May appear as additional consistent months, while the remaining consistent periods continue to exhibit decreases in emissions. Notably, from June to November, the two posterior datasets show an average decrease of 42.26% compared to the prior emissions, indicating a high probability of overestimation in the prior inventory for this region during that period.

...

**3.4 Impact of Formaldehyde Assimilation on $O_3$ Surface Concentration**

...

To more robustly substantiate this conclusion, it is necessary to examine whether similar features can also be identified in 2019. In that year, OMPS and TROPOMI satellite observations were assimilated independently to constrain NMVOC emissions. The posterior-prior increments from the OMPS- and TROPOMI-driven assimilations, together with the changes in MDA8 ozone ΔRMSE, are presented in Figure 9 of the Supplement. In NCP, March, May, and June are identified as consistent months, during which the ozone RMSE values decrease, with the most pronounced improvement occurring in June. In YRD, the consistent months are February, October, and November, where the ozone improvements are relatively limited but nevertheless show better agreement with ground-based observations. In PRD, the consistent months include January, February, and June-December; with the exception of August, September, and November, the ozone RMSE decreases in the other months, with notable improvements in June and July. In SCB, the two posterior datasets exhibit the highest level of consistency in 2019, with synchronous increases and decreases throughout the year. Ozone simulations in this region show better performance in all months except March and April, with particularly large improvements in June, July, and September-November, when the RMSE decreases by an average of 25.74%.

Across the four regions, 27 months are classified as consistent in 2019. Of these, 22 months exhibit improved ozone simulations, which corresponds to 81.48% of all consistent months, with both assimilations producing MDA8 ozone values closer to ground-based observations. This proportion differs from that of 2020 by only 0.23%, providing further evidence that ozone improvements are particularly significant in the months defined as consistent across the four regions.

...

**4 Summary and conclusion**

...

To further test the robustness of our approach, OMPS and TROPOMI satellite observations were independently assimilated to constrain NMVOC emissions for 2019 (Figure 7). The spatial distribution of formaldehyde hotspots is similar to 2020 but with overall higher concentrations. At the regional scale, most consistent months between OMPS- and TROPOMI-constrained results indicate that the prior inventory underestimates emissions in NCP and overestimates them in YRD, PRD, and SCB. Importantly, 22 of the 27 consistent months (81.48%) show reduced ozone RMSE, with the largest improvements in SCB, confirming that consistent cases are strongly associated with enhanced ozone simulation performance. These findings also lend greater confidence to the optimized NMVOC emissions during the consistent months in these regions.

**RC:** ***28) Define all acronyms at first use (e.g., NCP, MEIC, CEDS).***

AR: We thank the reviewer for this helpful comment. In the revised manuscript, we have ensured that all acronyms are defined at first use. The four study regions (e.g., North China Plain) and inventories such as CEDS and GFED are introduced with their full names at first mention. For MEIC, we used the acronym in the Abstract only as an example, since the full name is too long for that context, but the complete form Multi-resolution Emission Inventory for China (MEIC) is provided at its first appearance in the main text.

**Text in manuscript**

**Abstract**

...

As one of the world's largest NMVOC emitters, accurate emission inventories are essential for understanding and ~~controlling atmospheric pollution . Mainstream inventories are constructed using~~ mitigating air pollution in China. Commonly-used inventories (e.g., MEIC) are largely based on bottom-up ~~approaches, which cannot accurately reflect the spatiotemporal characteristics of NMVOCs~~methods, which often fail to capture the spatiotemporal variability of NMVOC emissions, resulting in ~~poor model outcomes~~significant model-observation mismatches.

...

Highly consistent increments are obtained in the North China Plain (May-June), the Yangtze River Delta and Pearl River Delta (January-March, ~~with the RMSE dropping from 0.52 to 0.37 $\times 10^{16}$ molec~~October-December), and the Sichuan Basin (January, June-December).

...

**1 Introduction**

...

NMVOCs are primarily released through anthropogenic activities, biogenic emissions, and biomass burning processes. Huge efforts have been devoted to constructing inventories recording these emissions in a bottom-up way, such as the global Community Emission Data System (CEDS) (Hao and Xie, 2018), the regional Multi-resolution Emission Inventory for China (MEIC) (Li et al., 2019), and the Model of Emissions of Gases and Aerosols from Nature v2.1 (MEGAN) (Guenther et al., 2012). ~~These NMVOC emission inventories coupled~~ For biomass burning, widely used inventories include the Global Fire Emissions Database (GFED) and the Fire INventory from NCAR (FINN) (Wiedinmyer et al., 2011). Coupled with chemical transport models like GEOS-Chem (Ito et al., 2007) and WRF-Chem (Azmi et al., 2022), ~~are capable of reproducing the complex processes including~~ these inventories are widely used to simulate transport, deposition, and chemical ~~reactions. This not only helps to better quantify the environmental impact~~ transformations of NMVOCs, ~~but also provides essential tools for predicting future trends and making emission reduction~~ supporting air quality assessments and emission control strategies.

**RC:** ***29) Ensure units, abbreviations, and mathematical notations are consistently applied.***

AR: We thank the reviewer for this comment. Units, abbreviations, and mathematical notations have been carefully reviewed and revised, and we have sought to apply them as consistently as possible throughout the manuscript.

**RC:** ***30) Review manuscript for grammar, sentence clarity, and fluency.***

AR: We thank the reviewer for this comment. We have carefully read through the manuscript to improve grammar, sentence clarity, and fluency, and have revised the text where needed to enhance readability.

## References


Azmi, S., Sharma, M., and Nagar, P. K.: NMVOC emissions and their formation into secondary organic aerosols over India using WRF-Chem model, Atmospheric Environment, 287, 119 254, 2022.

Billionnet, C., Gay, E., Kirchner, S., Leynaert, B., and Annesi-Maesano, I.: Quantitative assessments of indoor air pollution and respiratory health in a population-based sample of French dwellings, Environmental research, 111, 425–434, 2011.

Bo, Y., Cai, H., and Xie, S.: Spatial and temporal variation of historical anthropogenic NMVOCs emission inventories in China, Atmospheric Chemistry and Physics, 8, 7297–7316, 2008.

Boersma, K., Eskes, H., and Brinksma, E.: Error analysis for tropospheric NO2 retrieval from space, Journal of Geophysical Research: Atmospheres, 109, 2004.

Cao, H., Fu, T.-M., Zhang, L., Henze, D. K., Miller, C. C., Lerot, C., Abad, G. G., De Smedt, I., Zhang, Q., van Roozendael, M., et al.: Adjoint inversion of Chinese non-methane volatile organic compound emissions using space-based observations of formaldehyde and glyoxal, Atmospheric Chemistry and Physics, 18, 15 017–15 046, 2018.

Chance, K.: OMI/Aura Formaldehyde (HCHO) Total Column Daily L2 Global Gridded 0.25 degree x 0.25 degree V3, Greenbelt, MD, USA, Goddard Earth Sciences Data and Information Services Center (GES DISC), , accessed: [Data Access Date], 2014.

Cheng, J., Zhang, Y., Wang, T., Norris, P., Chen, W.-Y., and Pan, W.-P.: Thermogravimetric–Fourier transform infrared spectroscopy–gas chromatography/mass spectrometry study of volatile organic compounds from coal pyrolysis, Energy & Fuels, 31, 7042–7051, 2017.

Choi, J., Henze, D. K., Cao, H., Nowlan, C. R., González Abad, G., Kwon, H.-A., Lee, H.-M., Oak, Y. J., Park, R. J., Bates, K. H., et al.: An inversion framework for optimizing non-methane VOC emissions using remote sensing and airborne observations in Northeast Asia during the KORUS-AQ field campaign, Journal of Geophysical Research: Atmospheres, 127, e2021JD035 844, 2022.

Clarisse, L., Franco, B., Van Damme, M., Di Gioacchino, T., Hadji-Lazaro, J., Whitburn, S., Noppen, L., Hurtmans, D., Clerbaux, C., and Coheur, P.: The IASI NH 3 version 4 product: averaging kernels and improved consistency, Atmospheric Measurement Techniques Discussions, 2023, 1–31, 2023.

Cooper, M. J., Martin, R. V., Henze, D. K., and Jones, D.: Effects of a priori profile shape assumptions on comparisons between satellite NO 2 columns and model simulations, Atmospheric Chemistry and Physics, 20, 7231–7241, 2020.

Duncan, B. N., Yoshida, Y., Olson, J. R., Sillman, S., Martin, R. V., Lamsal, L., Hu, Y., Pickering, K. E., Retscher, C., Allen, D. J., et al.: Application of OMI observations to a space-based indicator of NOx and VOC controls on surface ozone formation, Atmospheric Environment, 44, 2213–2223, 2010.

González Abad, G., Vasilkov, A., Seftor, C., Liu, X., and Chance, K.: Smithsonian astrophysical observatory ozone mapping and profiler suite (SAO OMPS) formaldehyde retrieval, Atmospheric Measurement Techniques, 9, 2797–2812, 2016.

Guenther, A., Jiang, X., Heald, C. L., Sakulyanontvittaya, T., Duhl, T. a., Emmons, L., and Wang, X.: The Model of Emissions of Gases and Aerosols from Nature version 2.1 (MEGAN2. 1): an extended and updated framework for modeling biogenic emissions, Geoscientific Model Development, 5, 1471–1492, 2012.

Hao, Y. and Xie, S.: Optimal redistribution of an urban air quality monitoring network using atmospheric dispersion model and genetic algorithm, Atmospheric Environment, 177, 222–233, 2018.

He, Z., Li, G., Chen, J., Huang, Y., An, T., and Zhang, C.: Pollution characteristics and health risk assessment of volatile organic compounds emitted from different plastic solid waste recycling workshops, Environment international, 77, 85–94, 2015.

Ito, A., Sillman, S., and Penner, J. E.: Effects of additional nonmethane volatile organic compounds, organic nitrates, and direct emissions of oxygenated organic species on global tropospheric chemistry, Journal of Geophysical Research: Atmospheres, 112, 2007.

Jin, J., Segers, A., Lin, H. X., Henzing, B., Wang, X., Heemink, A., and Liao, H.: Position correction in dust storm forecasting using LOTOS-EUROS v2.1: grid-distorted data assimilation v1.0, Geoscientific Model Development, 14, 5607–5622, , URL https://gmd.copernicus.org/articles/14/5607/2021/, 2021.

Jin, J., Fang, L., Li, B., Liao, H., Wang, Y., Han, W., Li, K., Pang, M., Wu, X., and Lin, H. X.: 4DEnVar-based inversion system for ammonia emission estimation in China through assimilating IASI ammonia retrievals, Environmental Research Letters, 18, 034 005, 2023.

Jung, J., Choi, Y., Mousavinezhad, S., Kang, D., Park, J., Pouyaei, A., Ghahremanloo, M., Momeni, M., and Kim, H.: Changes in the ozone chemical regime over the contiguous United States inferred by the inversion of NOx and VOC emissions using satellite observation, Atmospheric research, 270, 106 076, 2022.

Kaiser, J., Jacob, D. J., Zhu, L., Travis, K. R., Fisher, J. A., González Abad, G., Zhang, L., Zhang, X., Fried, A., Crounse, J. D., et al.: High-resolution inversion of OMI formaldehyde columns to quantify isoprene emission on ecosystem-relevant scales: application to the southeast US, Atmospheric Chemistry and Physics, 18, 5483–5497, 2018.

Lee, J.-S.: Digital image enhancement and noise filtering by use of local statistics, IEEE transactions on pattern analysis and machine intelligence, pp. 165–168, 1980.

Lerner, J. C., Sanchez, E. Y., Sambeth, J. E., and Porta, A. A.: Characterization and health risk assessment of VOCs in occupational environments in Buenos Aires, Argentina, Atmospheric environment, 55, 440–447, 2012.

Li, L., Yang, W., Xie, S., and Wu, Y.: Estimations and uncertainty of biogenic volatile organic compound emission inventory in China for 2008–2018, Science of the Total Environment, 733, 139 301, 2020.

Li, M., Liu, H., Geng, G., Hong, C., Liu, F., Song, Y., Tong, D., Zheng, B., Cui, H., Man, H., et al.: Anthropogenic emission inventories in China: a review, Natl. Sci. Rev., 4, 834–866, 2017.

Li, M., Zhang, Q., Zheng, B., Tong, D., Lei, Y., Liu, F., Hong, C., Kang, S., Yan, L., Zhang, Y., et al.: Persistent growth of anthropogenic non-methane volatile organic compound (NMVOC) emissions in China during 1990–2017: drivers, speciation and ozone formation potential, Atmospheric Chemistry and Physics, 19, 8897–8913, 2019.

Liu, C., Xiao, Q., and Wang, B.: An ensemble-based four-dimensional variational data assimilation scheme. Part I: Technical formulation and preliminary test, Monthly Weather Review, 136, 3363–3373, 2008.

Miyazaki, K., Bowman, K. W., Yumimoto, K., Walker, T., and Sudo, K.: Evaluation of a multi-model, multi-constituent assimilation framework for tropospheric chemical reanalysis, Atmospheric Chemistry and Physics, 20, 931–967, 2020.

Nowlan, C. R., González Abad, G., Kwon, H.-A., Ayazpour, Z., Chan Miller, C., Chance, K., Chong, H., Liu, X., O'Sullivan, E., Wang, H., et al.: Global formaldehyde products from the Ozone Mapping and Profiler Suite (OMPS) nadir mappers on Suomi NPP and NOAA-20, Earth and Space Science, 10, e2022EA002 643, 2023.

Oomen, G.-M., Müller, J.-F., Stavrakou, T., De Smedt, I., Blumenstock, T., Kivi, R., Makarova, M., Palm, M., Röhling, A., Té, Y., et al.: Weekly derived top-down volatile-organic-compound fluxes over Europe from TROPOMI HCHO data from 2018 to 2021, Atmospheric Chemistry and Physics, 24, 449–474, 2024.

Palmer, P. I., Jacob, D. J., Chance, K., Martin, R. V., Spurr, R. J., Kurosu, T. P., Bey, I., Yantosca, R., Fiore, A., and Li, Q.: Air mass factor formulation for spectroscopic measurements from satellites: Application to formaldehyde retrievals from the Global Ozone Monitoring Experiment, Journal of Geophysical Research: Atmospheres, 106, 14 539–14 550, 2001.

Palmer, P. I., Jacob, D. J., Fiore, A. M., Martin, R. V., Chance, K., and Kurosu, T. P.: Mapping isoprene emissions over North America using formaldehyde column observations from space, Journal of Geophysical Research: Atmospheres, 108, 2003.

Pei, D., Wang, A., Shen, L., and Wu, J.: Research on the Emission of Biogenic Volatile Organic Compounds from Terrestrial Vegetation, Atmosphere, 16, 885, 2025.

Sakdapipanich, J. and Insom, K.: High-resolution gas chromatography-mass spectrometry, KGK Kautschuk Gummi Kunststoffe, 59, 382–387, 2006.

Sharma, S., Goel, A., Gupta, D., Kumar, A., Mishra, A., Kundu, S., Chatani, S., and Klimont, Z.: Emission inventory of non-methane volatile organic compounds from anthropogenic sources in India, Atmospheric Environment, 102, 209–219, 2015.

Shim, C., Wang, Y., Choi, Y., Palmer, P. I., Abbot, D. S., and Chance, K.: Constraining global isoprene emissions with Global Ozone Monitoring Experiment (GOME) formaldehyde column measurements, Journal of Geophysical Research: Atmospheres, 110, 2005.

Souri, A. H., Choi, Y., Jeon, W., Woo, J.-H., Zhang, Q., and Kurokawa, J.-i.: Remote sensing evidence of decadal changes in major tropospheric ozone precursors over East Asia, Journal of Geophysical Research: Atmospheres, 122, 2474–2492, 2017.

Souri, A. H., Nowlan, C. R., González Abad, G., Zhu, L., Blake, D. R., Fried, A., Weinheimer, A. J., Wisthaler, A., Woo, J.-H., Zhang, Q., et al.: An inversion of NO x and non-methane volatile organic compound (NMVOC) emissions using satellite observations during the KORUS-AQ campaign and implications for surface ozone over East Asia, Atmospheric Chemistry and Physics, 20, 9837–9854, 2020.

Stavrakou, T., Müller, J.-F., Bauwens, M., De Smedt, I., Lerot, C., Van Roozendael, M., Coheur, P.-F., Clerbaux, C., Boersma, K., Van Der A, R., et al.: Substantial underestimation of post-harvest burning emissions in the North China Plain revealed by multi-species space observations, Scientific Reports, 6, 32 307, 2016.

Wang, H., Wu, Q., Guenther, A. B., Yang, X., Wang, L., Xiao, T., Li, J., Feng, J., Xu, Q., and Cheng, H.: A long-term estimation of biogenic volatile organic compound (BVOC) emission in China from 2001–2016: the roles of land cover change and climate variability, Atmospheric Chemistry and Physics, 21, 4825–4848, 2021.

Wells, K., Millet, D., Payne, V., Vigouroux, C., Aquino, C., De Mazière, M., de Gouw, J., Graus, M., Kurosu, T., Warneke, C., et al.: Next-generation isoprene measurements from space: Detecting daily variability at high resolution, Journal of Geophysical Research: Atmospheres, 127, e2021JD036 181, 2022.

Wells, K. C., Millet, D. B., Payne, V. H., Deventer, M. J., Bates, K. H., de Gouw, J. A., Graus, M., Warneke, C., Wisthaler, A., and Fuentes, J. D.: Satellite isoprene retrievals constrain emissions and atmospheric oxidation, Nature, 585, 225–233, 2020.

Wiedinmyer, C., Akagi, S., Yokelson, R. J., Emmons, L., Al-Saadi, J., Orlando, J., and Soja, A.: The Fire INventory from NCAR (FINN): A high resolution global model to estimate the emissions from open burning, Geoscientific Model Development, 4, 625–641, 2011.

Wu, K., Yang, X., Chen, D., Gu, S., Lu, Y., Jiang, Q., Wang, K., Ou, Y., Qian, Y., Shao, P., et al.: Estimation of biogenic VOC emissions and their corresponding impact on ozone and secondary organic aerosol formation in China, Atmospheric Research, 231, 104 656, 2020.

Wu, N., Geng, G., Xu, R., Liu, S., Liu, X., Shi, Q., Zhou, Y., Zhao, Y., Liu, H., Song, Y., et al.: Development of a high-resolution integrated emission inventory of air pollutants for China, Earth System Science Data, 16, 2893–2915, 2024.

Xia, J., Zhou, Y., Fang, L., Qi, Y., Li, D., Liao, H., and Jin, J.: South Asia ammonia emission inversion through assimilating IASI observations, EGUsphere, 2025, 1–22, 2025.

Xing, Y., Wang, G., Zhang, T., Shen, F., Meng, L., Wang, L., Li, F., Zhu, Y., Zheng, Y., He, N., et al.: VOC detections with optical spectroscopy, Prog. Electromagn. Res, 173, 71–92, 2022.

Xue, R., Wang, S., Li, D., Zou, Z., Chan, K. L., Valks, P., Saiz-Lopez, A., and Zhou, B.: Spatio-temporal variations in NO2 and SO2 over Shanghai and Chongming Eco-Island measured by Ozone Monitoring Instrument (OMI) during 2008–2017, Journal of Cleaner Production, 258, 120 563, 2020.

Yuan, B., Hu, W., Shao, M., Wang, M., Chen, W., Lu, S., Zeng, L., and Hu, M.: VOC emissions, evolutions and contributions to SOA formation at a receptor site in eastern China, Atmospheric Chemistry and Physics, 13, 8815–8832, 2013.

Zhu, L., Jacob, D. J., Kim, P. S., Fisher, J. A., Yu, K., Travis, K. R., Mickley, L. J., Yantosca, R. M., Sulprizio, M. P., De Smedt, I., et al.: Observing atmospheric formaldehyde (HCHO) from space: validation and intercomparison of six retrievals from four satellites (OMI, GOME2A, GOME2B, OMPS) with SEAC 4 RS aircraft observations over the southeast US, Atmospheric chemistry and physics, 16, 13 477–13 490, 2016.

Zhu, L., Jacob, D. J., Keutsch, F. N., Mickley, L. J., Scheffe, R., Strum, M., González Abad, G., Chance, K., Yang, K., Rappenglück, B., et al.: Formaldehyde (HCHO) as a hazardous air pollutant: Mapping surface air concentrations from satellite and inferring cancer risks in the United States, Environmental Science & Technology, 51, 5650–5657, 2017.